SIAM J. Applied Dynamical Systems
Vol. 9, No. 4, pp. 1303–1347

Binocular Rivalry in a Competitive Neural Network with Synaptic Depression*

Zachary P. Kilpatrick† and Paul C. Bressloff‡

Abstract. We study binocular rivalry in a competitive neural network with synaptic depression. In particular, we consider two coupled hypercolums within primary visual cortex (V1), representing orientation selective cells responding to either left or right eye inputs. Coupling between hypercolumns is dominated by inhibition, especially for neurons with dissimilar orientation preferences. Within hypercolumns, recurrent connectivity is excitatory for similar orientations and inhibitory for different orientations. All synaptic connections are modifiable by local synaptic depression. When the hypercolumns are driven by orthogonal oriented stimuli, it is possible to induce oscillations that are representative of binocular rivalry. We first analyze the occurrence of oscillations in a space-clamped version of the model using a fast-slow analysis, taking advantage of the fact that depression evolves much slower than population activity. We then analyze the onset of oscillations in the full spatially extended system by carrying out a piecewise smooth stability analysis of single (winner-take-all) and double (fusion) bumps within the network. Although our stability analysis takes into account only instabilities associated with real eigenvalues, it identifies points of instability that are consistent with what is found numerically. In particular, we show that, in regions of parameter space where double bumps are unstable and no single bumps exist, binocular rivalry can arise as a slow alternation between either population supporting a bump.

Key words. neuronal network, hypercolumn, binocular rivalry, synaptic depression, piecewise-smooth dynamics

AMS subject classifications. 92C20, 37L15

DOI. 10.1137/100788872

1. Introduction.

Binocular rivalry concerns the phenomenon whereby perception switches back and forth between different images presented to either eye. Due to the supposed link to activity in the lateral geniculate nucleus (LGN) and the visual cortex, binocular rivalry continues to be an excellent way to obtain information about the human visual system [28, 59]. Psychophysical experiments are noninvasive and can provide a great deal of data about the response of the visual system to different characteristics of binocular stimuli. Currently, there are several open problems in binocular rivalry including the relationship between the type of stimuli and resulting perception, the neural sites encoding perception, and the neural connections that facilitate competition of stimuli.

Although binocular rivalry has been studied for hundreds of years, only recently have experimentalists clarified some of its specific statistical properties [7]. In 1965, Levelt proposed four characteristics of binocular rivalry which he had ascertained empirically: (i) increasing

*Received by the editors March 16, 2010; accepted for publication (in revised form) by B. Ermentrout September 23, 2010; published electronically December 2, 2010. This research was supported in part by the National Science Foundation (DMS-0813677) and by award KUK-C1-013-4 made by King Abdullah University of Science and Technology (KAUST).
http://www.siam.org/journals/siads/9-4/78887.html
†Department of Mathematics, University of Utah, Salt Lake City, UT 84112 (kilpatri@math.utah.edu).
‡Mathematical Institute, University of Oxford, 24-29 St. Giles', Oxford OX1 3LB, UK (bressloff@maths.ox.ac.uk).
The work of this author was partially supported by the Royal Society Wolfson Foundation.

the contrast of the stimulus in one eye increases the predominance of the stimulus in that eye; (ii) increasing the contrast in one eye does not affect average dominance time of that eye; (iii) increasing contrast in one eye increases the rivalry alternation rate; and (iv) increasing the contrast in both eyes increases the rivalry alternation rate [45]. Propositions (i), (iii), and (iv) together imply that when the contrast of a stimulus to one eye is increased, the length of time the other eye's stimulus spends in dominance will decrease. Following Levelt's study other independent experiments have verified this observation that the modulated stimulus will spend less time being suppressed [24, 46]. Bossink and colleagues used an apparatus and paradigm similar to that of Levelt and found that proposition (ii) did not hold for various types of stimuli [9]. A recent study also found that proposition (ii) holds only for a certain range of stimulus contrasts [10]. Interestingly, this is the proposition that is often contradicted by the results of various modeling studies of binocular rivalry that use reciprocal inhibition [41, 39, 25].

Recent psychophysical experiments have revealed properties additional to those supported by Levelt's work. First, it appears that the switching from one percept to the next occurs stochastically. Independent studies have verified that there is little or no correlation between one dominance time and the next [42, 10]. With this in mind, the relationships determined by Levelt can be considered the average perception of the subject over many trials. Also, there is a long standing theory that attention to a particular stimulus can prolong the dominance time of the attended stimulus [29]. Experimental evidence suggests that this correlation may hold true when the subject practices repeatedly [38, 17]. However, the nonattended stimulus will eventually appear in the observer's perception, no matter how strongly attention is focused on the other. The fact that attention can bias the outcomes of binocular rivalry suggests that higher level visual areas may play a modulatory role in the phenomenon [66]. Attention may increase the apparent contrast of the attended stimulus or simply boost the activity of one of two competing neural populations [17]. In addition, experiments have verified that the "tilt aftereffect" is still observed when vertical and tilted lines are rivalrous stimuli [64]; the tilt aftereffect is the phenomenon by which staring at a slightly tilted line will make a vertical line appear to be tilted in the opposite direction if viewed immediately after. Since the neural substrate of this phenomenon is known to reside in primary visual cortex (V1), this suggests that binocular rivalry can involve V1 [34]. Thus, without even recording activity signals from the brain, a great deal about the neural site of binocular rivalry can be learned from subjects reporting their perceptual responses to stimuli.

Several different methods of recording neural activity in subjects during binocular rivalry have also been employed in an effort to isolate the specific sites of its encoding. In monkeys, single electrode recordings have been employed to track electrical activity during binocular rivalry tasks [7]. Evidence has been found in the V1, V2, and V4 regions of visual cortex of an elevation in some cells' firing rates that corresponds well with the monkey's reported perception of a stimulus [44]. Thus, it appears that several areas of visual cortex may be involved. However, single unit recordings have yet to reveal changes in the firing rate of LGN neurons that correspond to the perceptual changes of binocular rivalry [43]. In humans, less invasive techniques such as scalp recording and functional magnetic resonance imaging (fMRI) have helped to localize brain regions whose activity reflects the experience of binocular rivalry. Visually evoked potentials measured on the scalp during a binocular rivalry task reveal that

potential waveforms associated with each stimulus possess a timecourse very closely linked to the subject's perceptual observation [13]. A number of fMRI studies have verified that there are changes in the blood oxygen level dependent (BOLD) signals in V1 that correspond to the perceived switching in stimulus dominance [51, 59, 40]. In addition, recent work has used fMRI of the BOLD signal to find correspondence between the activity in LGN and a human subject's percepts during binocular rivalry [28]. However, this may be due to functionally specific feedback connections from V1 to LGN that are possibly imposing activity fluctuations up the visual stream [33]. All of these results point to a number of possibilities as to the central visual area encoding binocular rivalry [7]. Some theories even propose that there may be a hierarchy of visual areas involved so that there is a competition between either eye's input as well as differing patterns [66, 60].

Since we will focus here on modeling binocular rivalry in V1, it is useful to describe some essential features of the functional architecture of V1. First, each neuron in V1 has a particular patch of the visual scene to which it responds, known as its classical receptive field [31, 32]. Stimuli outside a neuron's receptive field do not directly affect its activity. Second, most neurons in V1 respond preferentially to stimuli of a particular eye, right or left, which assigns their *ocular dominance* [31, 8, 48]. It has been suggested that neurons with different ocular dominance (one right and one left) may inhibit one another if they have nearby receptive fields [35]. As signals are relayed to higher areas of visual cortex, these two pathways are combined to process more complex stimuli. Third, most neurons in V1 are tuned to respond maximally when a stimulus of a particular orientation is in their receptive field [31, 16, 8]. This is known as a neuron's *orientation preference*, and the neuron will not be directly affected if a stimulus is sufficiently different from its preferred orientation. Finally, there is a great deal of evidence which suggests that, for a discrete patch of visual space, there exists a corresponding collection of neurons spanning the entire spectrum of orientation preferences that are packed together as a unit in V1, known as a *hypercolumn* [32, 61, 26]. Despite recent studies that have called into question the reality of the hypercolumn as a structure [30], there is certainly a periodic map of feature preferences in V1 that can be modeled quite cleanly with the idea of the hypercolumn [11]. Using multielectrode and optical imaging techniques, periodicity in orientation preference has been shown across V1 where each period corresponds to a coarse location in retinotopic space [32, 8]. Within this hypercolumn, neurons with sufficiently similar orientations will excite each other, and those with sufficiently different orientations will inhibit each other, which serves to sharpen a particular neuron's orientation preference [26, 5, 23]. Anatomical evidence suggests that interhypercolumn connections excite similar orientations [55, 3]. The functional relationship between stimulus feature preferences and synaptic connections within V1 suggests that V1 is a likely substrate of many simple examples of binocular rivalry such as those involving sinusoidal grating stimuli.

As a basic model example of binocular rivalry in V1, suppose that a horizontally oriented grating is presented to the left eye and a vertically oriented grating is presented to the right eye. This triggers rivalry due to the combination of orientation specific and ocular dominant cross-inhibition in V1 [5, 55, 7]. During left eye stimulus dominance, it is proposed that a group of the left eye neurons that respond to horizontal orientations are firing persistently, while right eye neurons are suppressed by cross-inhibitory connections. Of course, there may still be some low rate firing of the right eye neurons, but it will be less than the firing rate of

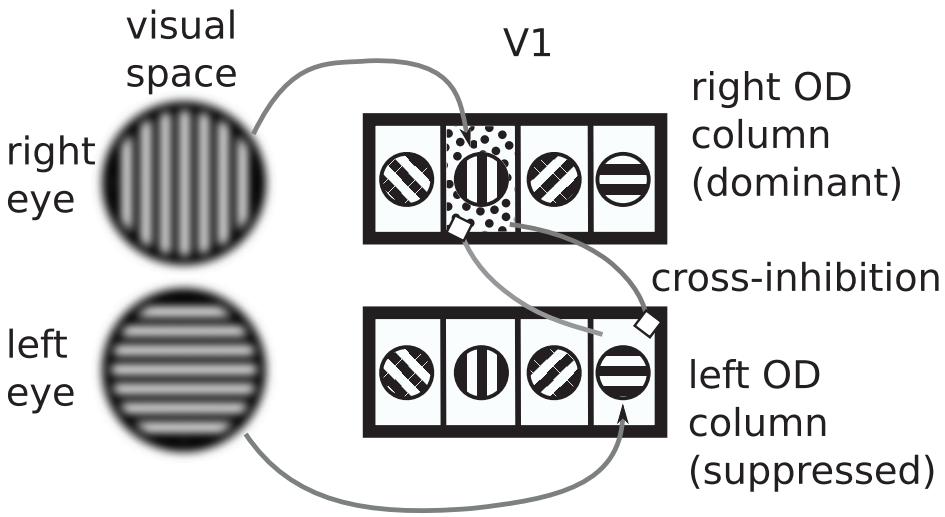

Figure 1. *Primary visual cortex* (V1) *response to rival grating stimuli consisting of a vertical (horizontal) grating presented to the right (left) eye. A snapshot in time is shown where the vertical orientation preference neurons fire persistently (polka dots) in the right OD column, while the horizontal orientation preference neurons in the left OD column are quiescent, even though they are receiving input. Vertically preferring neurons in the right OD column firing at a high rate project inhibition (white diamonds) to the horizontally preferring neurons in the left OD column to keep them from firing. In a winner-take-all (WTA) scenario, the plot would remain unchanged as time evolves, but in a binocular rivalry situation, a slow adaptive process would eventually cause the left OD column's horizontal orientation preference neurons to switch from suppressed to dominant.*

the left eye, horizontally tuned neurons [7]. Following this, some slow adaptive process causes a switch so that right eye, vertical orientation neurons fire persistently, suppressing the left eye neurons (see Figure 1). The cycle of left eye neural dominance along with right eye neural suppression followed by right eye neural dominance along with left eye neural suppression can continue indefinitely. This basic model of reciprocal inhibition paired with a slow adaptive process has often been used to phenomenologically model the neural substrate of binocular rivalry [24, 65, 54, 39, 58, 52]. In this paper, we extend these ideas by analyzing binocular rivalry in a spatially extended coupled hypercolumn model of V1 driven by oriented grating stimuli. While other types of stimuli may employ higher areas of visual cortex as neural substrates of binocular rivalry [66, 60], the precise connection between neural activity and more complex images such as a face or a house are not as well understood [7].

It remains an open question as to which slow adaptive process is most responsible for the eventual switching of one stimulus dominance to the other [52]. The mechanism of spike frequency adaptation has been suggested, since it can curtail excitatory activity in a single neuron [67, 39]. Spike frequency adaptation is the process by which a hyperpolarizing current is switched on due to a build-up of a certain ion, like calcium, within the cell due to repetitive firing [56]. The maximal firing rate of a neuron is lowered as a result. In the case of binocular rivalry, this may cause the dominant population to eventually drop its firing rate so that cross-inhibition suppressing the other population is then low enough for the suppressed

populations to rekindle its firing rate into dominance. Since the recently released population is not adapted, it can then remain in dominance and suppress the other population for a period of time roughly equal to the time constant of spike frequency adaptation [67, 39, 47]. Another proposed switching mechanism is that the inhibitory synapses from one eye's neurons to the other's undergo synaptic depression.[1] This is the process by which synaptic resources such as neurotransmitters, vesicles, and scaffolding proteins are exhausted due to their continuous use [63, 15]. If inhibitory synapses remain repeatedly active, due to one eye's neurons suppressing the other's, eventually most of those synapses' resources will be used up, the effect of inhibition will be weakened, and the suppressed population will escape [39, 52].

Previous modeling efforts have been helpful in determining the neural dynamics that may result from a specific slow adaptive process acting to produce rivalry. Some models employ heuristic forms that are unconcerned with the specific adaptive process leading to rivalrous switching, but they have been useful in delving deeper into the statistical properties of rivalrous oscillations [41, 25]. Other spiking neuron and firing rate models have employed more specific physiological forms for the slow adaptive process that leads to rivalrous switching [67, 39, 58, 66, 49, 52, 20, 53, 47]. In most cases a firing rate model appears sufficient to capture the elevation in spiking associated with the dominant stimulus. The dynamics of oscillations in such reciprocally inhibitory networks are often divided into two main categories—"escape" and "release" [65, 54, 52]. Escape is the occurrence of a suppressed neural population kindling activity above some threshold, which then allows it to dominate the population that was suppressing it. This should be contrasted with release, wherein a dominant neural population intrinsically reduces its activity below some threshold so that the suppressed population can be freed. One property that has been observed across all theoretical models of binocular rivalry is that increasing the stimulus strength to both populations leads to a decrease (increase) in dominance times when oscillations occur via escape (release). Levelt proposition (iv) thus suggests that rivalrous oscillations in a network model should arise via an escape mechanism [45, 24, 9, 46, 14]. Laing and Chow [39] studied a reduced firing rate model of binocular rivalry using spike frequency adaptation and depression individually or together. (Such a model was derived from a more detailed, spatially extended spiking neuron model.) They found many paradigms where dominance times depended nonmonotonically on the strength of input. This indicates a mixture of escape and release mechanisms at work in their model, depending on the stimulus strength range. Taylor, Cottrell, and Kristan studied a simpler model where depression is the only slow adaptive process for switching and the firing rate function is Heaviside [58]. They found, exclusively, that increasing stimulus strength decreased dominance time, indicating an escape mechanism. More recently, Shpiro et al. have systematically compared the form of rivalrous oscillations in a variety of firing rate models with spike frequency adaptation and/or synaptic depression [52, 53]. One common relationship they found across most models was that when the strength of both stimulus inputs was low, if binocular rivalry existed, it was through a release mechanism, whereas at higher stimulus strengths, binocular rivalrous oscillations usually appeared via an escape mechanism. These authors also explored the role

[1] More precisely, synaptic depression tends to be associated only with excitatory synapses, so that in our simplified model depressing inhibitory connections would have to be mediated by excitatory connections innervating local interneurons, for example.

of noise in accounting for dominance time statistics. Finally, Curtu et al. have carried out a rigorous mathematical analysis of the adaptation-based switching mechanism in a reciprocal inhibitory model with slow adaptation [20].

In this paper, we extend previous modeling studies by analyzing binocular rivalry in V1 using a spatially extended firing rate model with depressing synapses. In particular, we consider a competitive neural network model of binocular rivalry in which a pair of hypercolumns for the left and right eyes, respectively, are coupled together with depressing local and cross-inhibitory synapses [5, 11]; see Figure 1. Laing and Chow [39] considered a coupled hypercolumn model similar to ours which includes both adaptation and depression in a network of spiking neurons. However, they carried out a rigorous analysis only on a reduced rate-based system with adaptation. Rivalry effects in a spatially extended model with spike frequency adaptation have also been examined in a prior study by Loxley and Robinson [47], in which rivalrous stimuli are presented to a single one-dimensional network. While there has been some previous work studying synaptic depression as the sole mechanism for rivalry [58, 52], none has studied the onset of rivalrous oscillations by analyzing bifurcations of stationary bump solutions in a spatially extended system. In our model, we take the firing rate function to be a Heaviside, since this allows for analytical tractability. However, we also investigate numerically to what extent our results persist when the firing rate function is taken to be a smooth sigmoid. The choice of a Heaviside is also motivated by the result found in [58], namely, that a depressing network with a Heaviside firing rate supports only escape rivalry mechanisms, which has more biological support [45, 46]. A Heaviside firing rate function also leads to interesting dynamical phenomena, due to the resultant piecewise-smooth nature of the system. It could be argued that the dynamics of networks with Heaviside nonlinearities are unrealistic from a neurophysiological perspective. However, many studies of neuronal networks involving the high-gain limit of the sigmoid function, including Amari's [2], have proven useful in developing analytic relationships between parameters and the behaviors of standing and traveling wave solutions (see [19] for review). Moreover, it is possible to extend results obtained in networks with Heaviside nonlinearities to those with sigmoidal nonlinearities, using singular perturbation methods [50] or fixed point theorems [22]. One final point regarding Heaviside nonlinearities is that nongeneric behavior witnessed in this case may indicate that dynamical behavior observed in a corresponding network with sigmoid firing rate functions may be singular in the high-gain limit. Specifically, we have previously found that the range in which linear stability analysis is valid for standing bumps in networks with nonlinear adaptation becomes vanishingly small as the sigmoid gain is taken to infinity [12, 37].

The structure of the paper is as follows. We introduce the model in section 2 and analyze a space clamped version of the model in section 3. Similar to a previous study with both adaptation and depression [39], we derive explicit formulae for the relation between dominance times and the parameters of the model. Thus, we are able to compare the results of our model with the Levelt propositions given above. In particular, we show that in our model rivalrous oscillations occur exclusively via an escape mechanism resulting in dominance times that are consistent with Levelt proposition (iv). We also study the effects of additive noise on the statistics of dominance times and show that the latter is more consistent with experimental data when the depression variables rather than the activity variables are noise-driven. In section 4, we analyze binocular rivalry in the full spatially extended model by considering

dynamical instabilities of stationary bump solutions. We consider the existence of both winner-take-all (WTA) solutions, represented by a single bump of activity persisting in a single population, and solutions where both populations support persistent bumps. We then analyze the linear stability of these solutions by taking into account the piecewise-smooth nature of the neural field equations arising from the use of a Heaviside firing rate function. As in previous studies [12, 37], it is necessary to keep track of the sign of perturbations of the bump boundary in order to characterize instabilities accurately. Finally, in section 5 we simulate the spatially extended system using a numerical approximation scheme and compare it with the results of our stability analysis.

2. Coupled hypercolumn model. We consider a neuronal network subdivided into two distinct populations (hypercolumns), one responding to the left eye and the other to the right eye; see Figure 1. (A similar network architecture was considered by Laing and Chow [39].) Each eye's local and cross-population synapses experience synaptic depression [63, 62]. This is an extension of recent work, which has considered synaptic depression in a single population [12, 37]. Thus, the network in the most general form is described by the system of equations

$$\tau \frac{\partial u_L(\theta,t)}{\partial t} = -u_L(\theta,t) + w_l * (q_L f(u_L)) + w_c * (q_R f(u_R)) + I_L(\theta), \tag{2.1a}$$

$$\tau \frac{\partial u_R(\theta,t)}{\partial t} = -u_R(\theta,t) + w_l * (q_R f(u_R)) + w_c * (q_L f(u_L)) + I_R(\theta), \tag{2.1b}$$

$$\frac{\partial q_j(\theta,t)}{\partial t} = \frac{1-q_j(\theta,t)}{\alpha} - \beta q_j(\theta,t) f(u_j(\theta,t)), \quad j = L, R, \tag{2.1c}$$

where

$$w_m * (q_j f(u_j)) = \int_{-\pi/2}^{\pi/2} w_m(\theta,\theta') q_j(\theta',t) f(u_j(\theta',t)) \mathrm{d}\theta', \quad j = L, R, \quad m = l, c.$$

Equations (2.1a) and (2.1b) describe the evolution of the synaptic current or drive $u_L(\theta,t)$ and $u_R(\theta,t)$ of neurons with orientation preference $\theta \in [-\pi/2, \pi/2]$ responding either to left (L) or right (R) eye inputs $I_j(\theta)$, $j = L, R$. The nonlinear function f represents the mean firing rate of a local population and is usually taken to be a smooth, bounded, monotonic function such as a sigmoid [68, 50, 22]

$$f(u) = \frac{1}{1+\mathrm{e}^{-\eta(u-\kappa)}}, \tag{2.2}$$

with gain η and threshold κ. However, in order to explicitly compute solutions of interest, it will be convenient to consider the high-gain limit $\eta \to \infty$ of (2.2) such that f becomes a Heaviside function [2, 50, 18, 19, 27, 36]:

$$f(u) = \Theta(u-\kappa) = \begin{cases} 0 & \text{if } u < \kappa, \\ 1 & \text{if } u > \kappa. \end{cases} \tag{2.3}$$

The strength of connections between neurons within a single eye's population (local) and from one population to another (cross) are specified by the weight functions $w_l(\theta,\theta')$ and

$w_c(\theta,\theta')$, respectively. A typical weight distribution within the hypercolumn or "ring" model is a harmonic function dependent on the difference in orientations [5, 11, 69]. Thus, for our studies of simple grating based binocular rivalry, we will employ the functions

$$w_m(\theta,\theta') = w_m(\theta-\theta') = w_0^m + w_2^m \cos(2(\theta-\theta')), \quad m = l, c, \tag{2.4}$$

where w_0^m is the mean strength of connectivity and w_2^m is the orientation specific strength. The harmonic function $\cos(2(\theta-\theta'))$ of orientation preference difference is well matched to experimental studies of synaptic interaction of nearby neurons based on their orientation preference [23]. Depressing synapses are incorporated into the model in the form of a presynaptic scaling factor $q_j(\theta,t)$ evolving according to (2.1c). The factor $q_j(\theta,t)$ can be interpreted as a measure of available presynaptic resources, which are depleted at a rate βqf [62, 57, 4] and are recovered on a timescale specified by the constant α. Specifically, we will study the effect of slow short-term synaptic depression (experimentally shown to recover over 5–10s [63, 15]). Slow short-term synaptic depression has been implicated as a mechanism for contrast adaptation in V1 due to its comparable recovery timescale of 5–10s [63]. Thus, there is evidence for participation of this slower depression in processes of V1 in addition to faster short-term synaptic depression, which recovers on timescales of roughly 200–800ms [1, 63]. Finally, we fix the temporal scale of the network by setting $\tau = 1$. The membrane time constant is typically around 10ms, while the range of synaptic connections and specifically the size of a hypercolumn within the visual cortex is on the order of 1mm.

3. Oscillations in the space-clamped system. In this section we analyze oscillations in a space-clamped (θ-independent) version of our model. That is, we take the inputs I_L and I_R from both eyes to be homogeneous in the variable θ. While stimuli used in binocular rivalry experiments often have a preferred orientation to either eye, it is indeed possible to evoke the rivalry percept without such a specification [6]. Taking the weight functions to be given by the simple sum of harmonics (2.4) and specifying that solutions be homogeneous in θ, the system (2.1) becomes

$$\begin{aligned}
\dot{u}_L(t) &= -u_L(t) + \bar{w}_l q_L(t) f(u_L(t)) + \bar{w}_c q_R(t) f(u_R(t)) + I_L,\\
\dot{u}_R(t) &= -u_R(t) + \bar{w}_l q_R(t) f(u_R(t)) + \bar{w}_c q_L(t) f(u_L(t)) + I_R,\\
\dot{q}_j(t) &= (1-q_j(t))/\alpha - \beta q_j(t) f(u_j(t)), \quad j = L, R,
\end{aligned} \tag{3.1}$$

where

$$\bar{w}_m = \int_{-\pi/2}^{\pi/2} w_m(\theta')\mathrm{d}\theta', \quad m = l, c, \tag{3.2}$$

denotes the average strength of connectivity for either weight function. We will prescribe that $\bar{w}_c < 0$ so the cross connections are "inhibition-dominated," as this has been a suggested mechanism of binocular rivalry [35]. An extensive numerical study of equilibria of a system similar to (3.1) has been carried out when f is sigmoidal [52]. Thus, for the majority of this section, we will proceed analytically by examining the behavior of the system (3.1) in the case that f is the Heaviside function (2.3). In this case, we can compute any equilibria explicitly. Moreover, a fast-slow analysis can be used to determine the residence times spent with either

the left or right eye being dominant. In addition, we explore the effects that include additive noise in the equations for the activity variables $u_{L,R}$ as well as the depression variables $q_{L,R}$. It has been shown that including noise in reciprocally inhibitory networks with slow adaptation can lead to oscillation dominance times with gamma distribution statistics, as witnessed in psychophysical experiments of binocular rivalry [46, 52, 49]. Finally, we briefly study the equilibria and oscillations of the space-clamped system in the case of a smooth sigmoid firing rate function. We do not develop extensive analytical expressions relating parameters to steady states and switching times as in the Heaviside case, but we are able to study numerically how the steepness of the sigmoid affects the underlying dynamics.

3.1. Equilibria of network with Heaviside firing rate. We will follow reasoning similar to that of Laing and Chow [39], who used Heaviside functions to analyze binocular rivalry in a coupled hypercolumn model with spike frequency adaptation rather than synaptic depression. The dynamics of the system (3.1) can be characterized in terms of some simple parametric inequalities, specifying whether the system oscillates or settles into a steady state. A similar analysis was carried out by Taylor, Cottrell, and Kristan in a version of the network (3.1) without any local connections and a fixed synaptic depression strength [58]. Here, we will study the effect that including a local connectivity term $\bar{w}_l$ has upon the network dynamics. Of course, we are interested in the parameter regimes in which the system oscillates, since this is indicative of binocular rivalry. In these parameter regimes, we will compare the model with experimentally determined relations of input strength to dominance times [45, 9]. We also extend the work of [58] by examining dominance time dependence upon synaptic depression strength β and time constant α.

There are several different possible steady states, whose existence mainly depends on the strength of the input to either population. First, the off state given by $(u_L, u_R, q_L, q_R) = (I_L, I_R, 1, 1)$ occurs when $I_L, I_R < \kappa$, which implies that the input is not strong enough to activate either population. Second, the both-on or fusion state

$$u_j = \frac{\bar{w}_l + \bar{w}_c}{1+\alpha\beta} + I_j, \qquad q_j = \frac{1}{1+\alpha\beta}, \quad j = L, R, \tag{3.3}$$

occurs when $I_L, I_R > \kappa - (\bar{w}_l + \bar{w}_c)/(1+\alpha\beta)$. This case is more likely for very strong depression (β large), since cross-inhibition will be weak, or when the local connections are strong and excitation-dominated. The third type of equilibrium is the winner-take-all (WTA), where one population dominates the other. For example, if the left eye population is dominant, then

$$\begin{aligned} u_L &= \frac{\bar{w}_l}{1+\alpha\beta} + I_L, \quad u_R = \frac{\bar{w}_c}{1+\alpha\beta} + I_R, \\ q_L &= \frac{1}{1+\alpha\beta}, \qquad\qquad q_R = 1, \end{aligned} \tag{3.4}$$

which can be transformed to the right eye dominant case by interchanging L and R. For the steady state (3.4) to exist, we require

$$I_L > \kappa - \frac{\bar{w}_l}{1+\alpha\beta}, \quad I_R < \kappa - \frac{\bar{w}_c}{1+\alpha\beta}.$$

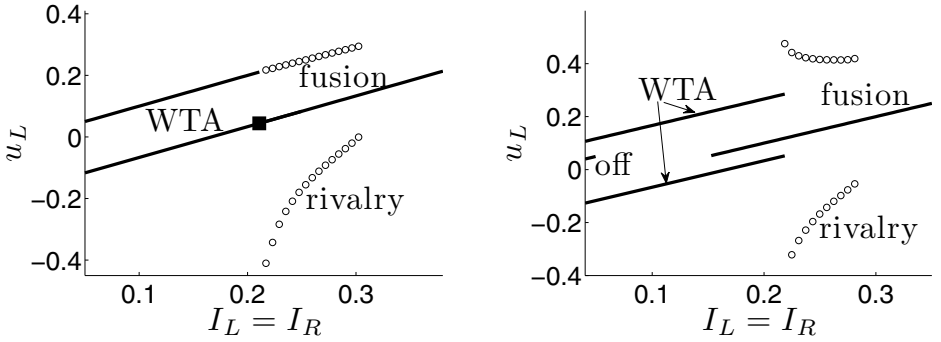

Figure 2. *Equilibria of the left population u_L as a function of the input amplitude $I_L = I_R$ to both populations. Solid lines represent stable states, whereas circles represent maximum and minimum of rivalrous oscillations. (Left) For no local connections, $\bar{w}_l = 0$, we find a bistable region, where rivalry coexists with a stable fusion state. Lower fixed point is the suppressed population of the WTA solution left of the black square and a fusion state to the right. (Right) When local connections are nonzero, $\bar{w}_l = 0.4$, there are regions of off/WTA bistability, WTA/fusion bistability, and fusion/rivalry bistability. Other parameters are $\kappa = 0.05$, $\alpha = 500$, $\beta = 0.01$, and $\bar{w}_c = -1$.*

This will occur in the presence of weak depression (β small) and strong cross-inhibition such that depression cannot exhaust the dominant hold one population has on the other.

The local stability of each equilibrium can be determined by calculating the general Jacobian for the system (3.1) in the case that $f(u) \equiv \Theta(u - \kappa)$ and $u_L, u_R \neq \kappa$:

$$\mathcal{J}(u_L, u_R, q_L, q_R) = \begin{pmatrix} -1 & 0 & \bar{w}_l\Theta(u_L - \kappa) & \bar{w}_c\Theta(u_R - \kappa) \\ 0 & -1 & \bar{w}_c\Theta(u_L - \kappa) & \bar{w}_l\Theta(u_R - \kappa) \\ 0 & 0 & -(\alpha^{-1} + \beta\Theta(u_L - \kappa)) & 0 \\ 0 & 0 & 0 & -(\alpha^{-1} + \beta\Theta(u_R - \kappa)) \end{pmatrix}. \tag{3.5}$$

It is straightforward to show that the eigenvalues of this Jacobian for a general equilibrium (excluding cases where $u_L = \kappa$ or $u_R = \kappa$) are

$$\lambda = -1, \quad -(\alpha^{-1} + \beta\Theta(u_L - \kappa)), \quad -(\alpha^{-1} + \beta\Theta(u_R - \kappa)), \tag{3.6}$$

which are all negative, regardless of the values u_L and u_R. Therefore, all steady states of the system (3.1) are stable. It follows that a limit cycle corresponding to a binocular rivalry state cannot arise from the destabilization of an equilibrium via a standard Hopf bifurcation. Indeed, we find that a limit cycle corresponding to an oscillating rivalrous state surrounds a stable fusion state, as illustrated in Figure 2. It can be seen that as the amplitude of the inputs $I_L = I_R$ is varied, the system (3.1) exhibits bistability between fusion/rivalry states, between off/WTA states, and between WTA/fusion states (when $\bar{w}_l \neq 0$). Such bistability has seldom been observed in other models of binocular rivalry. We point out here that these two bistable regimes were not observed in the study of the network (3.1) by Taylor, Cottrell, and Kristan due to their setting $\bar{w}_l = 0$. In [52], it was shown that Wilson's model [66] of binocular rivalry supports a WTA/rivalry bistable state. Their bifurcation analysis of the

Laing and Chow model did not exhibit bistability, perhaps owing to the fact that it included no recurrent excitation. Since the occurrence of oscillations cannot be studied using standard bifurcation theory, we will follow Laing and Chow [39] by assuming that we are in a regime where oscillations exist and characterize the dominance times by exploiting the separation in timescales between synaptic depression and neural activity, that is, $\alpha \gg 1$.

In order to appropriately study rivalry in the space-clamped system (3.1), it is important to understand the mechanism that will generate switching between one population dominating and then the other. As we have discussed, reciprocally inhibitory networks support oscillations resulting from two main types of mechanism—escape and release [65, 54, 20]. The competitive network with synaptic depression (3.1) that we study supports oscillations generated by escape only when the firing rate function is Heaviside, assuming the activity terms $u_{L,R}$ act much quicker than the depression terms $q_{L,R}$. This should be clear in the case $\bar{w}_l = 0$, but we wish to show this as well in the case $\bar{w}_l > 0$. We argue the network does not support release by a contradiction argument in the case where $I_L = I_R$ (this easily extends to the case where $I_L \neq I_R$). In oscillations generated by either escape or release, when the left population dominates,

$$u_L \approx \bar{w}_l q_L + I_L > \kappa \qquad \text{and} \qquad u_R \approx \bar{w}_c q_L + I_R < \kappa,$$

where we assume u_L and u_R relax to a slow manifold quite quickly. During oscillations generated by release, we expect a switch in dominance to occur by u_L dropping below threshold, allowing the release of u_R. At this point,

$$\bar{w}_l q_L + I_L = \kappa \qquad \Longrightarrow \qquad I_L = \kappa - \bar{w}_l q_L,$$

implying $I_L < \kappa$ since $\bar{w}_l > 0$. Thus, $I_R = I_L < \kappa$ as well, but for u_R to now spring above threshold, we must have $I_R > \kappa$, which is a contradiction. Thus, the system (3.1) will not support oscillations generated by a release mechanism in the case of a Heaviside firing rate and slow depression dynamics. Based on this result, and previous work, it seems that firing rate models of binocular rivalry must employ either spike frequency adaptation or a sigmoidal firing rate function with synaptic depression to generate oscillations through a release mechanism [20]. Thus, we have extended the results of [58] to show there is a broader class of competitive neural network models with synaptic depression that does not support release. In light of this, we perform our analysis of the relationship of dominance times to parameter under the assumption that the oscillation is generated by an escape mechanism.

Suppose that the system has settled onto a limit cycle as plotted in Figure 3 and that it is at the point where u_L has just escaped suppression by u_R. Since both u_L and u_R equilibrate quickly compared with q_L and q_R, it follows that

$$u_L(t) = \bar{w}_l q_L(t) + I_L, \qquad u_R(t) = \bar{w}_c q_L(t) + I_R. \tag{3.7}$$

We can also solve explicitly for $q_L(t)$ and $q_R(t)$ using the equations

$$\dot{q}_L = (1 - q_L)/\alpha - \beta q_L, \qquad \dot{q}_R = (1 - q_R)/\alpha. \tag{3.8}$$

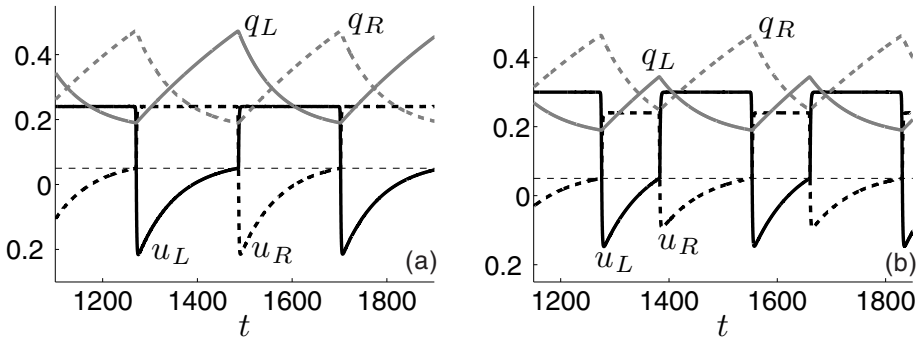

Figure 3. *Oscillatory solutions of the space-clamped system (3.1) for a Heaviside activation function (2.3). (Left) Plot against time of the activities u_L (solid black) and u_R (dashed black) with the depression variables q_L (solid grey) and q_R (dashed grey) when inputs are the same to both populations so that $I_L = I_R = 0.24$. This leads to an oscillation wherein the dominance times ($T_L = T_R \approx 210$) are equivalent for each percept. (Right) Plot against time of the activities u_L, u_R and depression variables q_L, q_R when inputs are different so that $I_L = 0.30$ and $I_R = 0.24$. This leads to an oscillation wherein the dominance times ($T_L \approx 170$, $T_R \approx 105$) are different for each percept. Other parameters are $\bar{w}_l = 0$, $\bar{w}_c = -1$, $\kappa = 0.05$, $\alpha = 500$, and $\beta = 0.01$.*

Assuming the initial conditions $q_L(0) = q_L^s$ and $q_R(0) = q_R^d$, we have

$$q_L(t) = \frac{1}{1+\alpha\beta} + \left(q_L^s - \frac{1}{1+\alpha\beta}\right) \mathrm{e}^{-(1+\alpha\beta)t/\alpha}, \tag{3.9}$$

$$q_R(t) = 1 - (1 - q_R^d)\mathrm{e}^{-t/\alpha} \tag{3.10}$$

for $t \in (0, T_L)$, where T_L is the dominance time of the left eye. Therefore, when the left eye population is suppressing the right eye population, the dynamics of the input currents are explicitly

$$u_L(t) = \bar{w}_l \left(\frac{1}{1+\alpha\beta} + \left(q_L^s - \frac{1}{1+\alpha\beta}\right) \mathrm{e}^{-(1+\alpha\beta)t/\alpha} \right) + I_L, \tag{3.11}$$

$$u_R(t) = \bar{w}_c \left(\frac{1}{1+\alpha\beta} + \left(q_L^s - \frac{1}{1+\alpha\beta}\right) \mathrm{e}^{-(1+\alpha\beta)t/\alpha} \right) + I_R. \tag{3.12}$$

At the time $t = T_L$, the synaptic drive u_R will escape from u_L's dominance by reaching threshold, that is, $u_R(T_L) = \kappa$. This generates the equation

$$\kappa = \bar{w}_c \left(\frac{1}{1+\alpha\beta} + \left(q_L^s - \frac{1}{1+\alpha\beta}\right) \mathrm{e}^{-(1+\alpha\beta)T_L/\alpha} \right) + I_R. \tag{3.13}$$

Note that although $u_L(T_L) > \kappa$, u_L will drop below threshold much more rapidly than the timescale of the q_j's due to cross-inhibition. Hence, we can make the approximation $T_L^* \approx T_L$, where $u_L(T_L^*) = \kappa$.

In the next phase of the oscillation

$$u_L(t) = \bar{w}_c q_R(t) + I_L, \qquad u_R(t) = \bar{w}_l q_R(t) + I_R, \tag{3.14}$$

with

$$\dot{q}_L = (1 - q_L)/\alpha, \qquad \dot{q}_R = (1 - q_R)/\alpha - \beta q_R. \tag{3.15}$$

Assuming the new set of initial conditions $q_L(T_L) = q_L^d$ and $q_R(T_L) = q_R^s$, we now have

$$q_L(t) = 1 - (1 - q_L^d)\mathrm{e}^{(T_L - t)/\alpha}, \tag{3.16}$$

$$q_R(t) = \frac{1}{1+\alpha\beta} + \left(q_R^s - \frac{1}{1+\alpha\beta}\right)\mathrm{e}^{(1+\alpha\beta)(T_L - t)/\alpha} \tag{3.17}$$

for $t \in (T_L, T_L + T_R)$, where T_R is the dominance time of the right eye. Therefore, when the right eye population is suppressing the left eye population, the dynamics of the input currents are approximately described by

$$u_L(t) = \bar{w}_c\left(\frac{1}{1+\alpha\beta} + \left(q_R^s - \frac{1}{1+\alpha\beta}\right)\mathrm{e}^{(1+\alpha\beta)(T_L - t)/\alpha}\right) + I_L, \tag{3.18}$$

$$u_R(t) = \bar{w}_l\left(\frac{1}{1+\alpha\beta} + \left(q_R^s - \frac{1}{1+\alpha\beta}\right)\mathrm{e}^{(1+\alpha\beta)(T_L - t)/\alpha}\right) + I_R. \tag{3.19}$$

Finally, at $t = T_L + T_R$, u_L will escape from u_R's dominance such that $u_L(T_L + T_R) = \kappa$. This generates the equation

$$\kappa = \bar{w}_c\left(\frac{1}{1+\alpha\beta}\left(q_R^s - \frac{1}{1+\alpha\beta}\right)\mathrm{e}^{-(1+\alpha\beta)T_R/\alpha}\right) + I_L. \tag{3.20}$$

At this point, $u_R > \kappa$, but u_R will rapidly drop below threshold so that $u_R(T_R^*) = \kappa$ with $T_R^* \approx T_R$.

Using (3.9), (3.10), (3.16), and (3.17), we have four equations for the four unknown initial conditions of the depression variables:

$$q_L^s = 1 - (1 - q_L^d)\mathrm{e}^{-T_R/\alpha}, \tag{3.21}$$

$$q_R^s = 1 - (1 - q_R^d)\mathrm{e}^{-T_L/\alpha}, \tag{3.22}$$

$$q_L^d = \frac{1}{1+\alpha\beta} + \left(q_L^s - \frac{1}{1+\alpha\beta}\right)\mathrm{e}^{-(1+\alpha\beta)T_L/\alpha}, \tag{3.23}$$

$$q_R^d = \frac{1}{1+\alpha\beta} + \left(q_R^s - \frac{1}{1+\alpha\beta}\right)\mathrm{e}^{-(1+\alpha\beta)T_R/\alpha}. \tag{3.24}$$

We can solve these explicitly for q_L^s and q_R^s in terms of the parameters α, β and the dominance times T_L, T_R as

$$q_L^s = \frac{\left(1 - \mathrm{e}^{-T_R/\alpha} + \frac{1}{1+\alpha\beta}\left(1 - \mathrm{e}^{-(1+\alpha\beta)T_L/\alpha}\right)\mathrm{e}^{-T_R/\alpha}\right)}{\left(1 - \mathrm{e}^{-(1+\alpha\beta)T_L/\alpha}\mathrm{e}^{-T_R/\alpha}\right)}, \tag{3.25}$$

$$q_R^s = \frac{\left(1 - \mathrm{e}^{-T_L/\alpha} + \frac{1}{1+\alpha\beta}\left(1 - \mathrm{e}^{-(1+\alpha\beta)T_R/\alpha}\right)\mathrm{e}^{-T_L/\alpha}\right)}{\left(1 - \mathrm{e}^{-(1+\alpha\beta)T_R/\alpha}\mathrm{e}^{-T_L/\alpha}\right)}. \tag{3.26}$$

Substituting (3.25) and (3.26) into (3.13) and (3.20) then gives

$$\kappa = \bar{w}_c\left(\frac{1}{1+\alpha\beta}+\left(\left(1-\mathrm{e}^{-T_R/\alpha}+\frac{1}{1+\alpha\beta}\left(1-\mathrm{e}^{-(1+\alpha\beta)T_L/\alpha}\right)\mathrm{e}^{-T_R/\alpha}\right)\right.\right.$$
$$\left.\left.\times\left(1-\mathrm{e}^{-(1+\alpha\beta)T_L/\alpha}\mathrm{e}^{-T_R/\alpha}\right)^{-1}-\frac{1}{1+\alpha\beta}\right)\mathrm{e}^{-(1+\alpha\beta)T_L/\alpha}\right)+I_R, \tag{3.27}$$

$$\kappa = \bar{w}_c\left(\frac{1}{1+\alpha\beta}+\left(\left(1-\mathrm{e}^{-T_L/\alpha}+\frac{1}{1+\alpha\beta}\left(1-\mathrm{e}^{-(1+\alpha\beta)T_R/\alpha}\right)\mathrm{e}^{-T_L/\alpha}\right)\right.\right.$$
$$\left.\left.\times\left(1-\mathrm{e}^{-(1+\alpha\beta)T_R/\alpha}\mathrm{e}^{-T_L/\alpha}\right)^{-1}-\frac{1}{1+\alpha\beta}\right)\mathrm{e}^{-(1+\alpha\beta)T_R/\alpha}\right)+I_L. \tag{3.28}$$

A numerical root finding algorithm can be used to solve for the dominance times T_L and T_R in terms of the parameters $\alpha, \beta, \kappa, \bar{w}_c$ and the input strengths I_L and I_R. We show examples of the dependence of these dominance times on a common drive strength to both populations $I_L = I_R = I_B$ and a modulation of input I_L, while keeping I_R constant in Figure 4. Taylor, Cottrell, and Kristan only studied the effect changing input strengths has on dominance times in the case $I_L = I_R = I_B$ [58]. Recall that Levelt proposition (iv) states increasing contrast (stimulus strength) to both eyes increases alternation rate, which is corroborated by $T_L = T_R = T_B$ being a decreasing function of I_B in Figure 4(a). Also, both propositions (i) and (iii) are in agreement with Figure 4(b), since increasing I_L leads to lower values of both T_L and T_R and the ratio $T_L/(T_L+T_R)$ increases as well. However, the Levelt proposition (ii) states increasing input to one eye does not change that eye's average dominance, but we find in Figure 4(b) that T_L decreases slightly. Indeed, previous experiments have produced results at odds with proposition (ii), finding that the statement may depend on specific contrast ranges of stimuli [9]. Comparing this with Laing and Chow's analysis of a firing rate model with depression and adaptation, we see qualitative similarity with dominance times being a decreasing function of input strength for symmetric and asymmetric inputs [39]. We find that this relation holds for $I_L > I_R$ as well. Interestingly, as our analytical results indicate, the dominance times do not depend at all on the strength of local connections $\bar{w}_l$, which we verified numerically as well. In [52], it was also shown that recurrent connections are not needed at all in order to produce the competition dynamics of rivalry in a network with synaptic depression. We extend [58] by also allowing synaptic depression strength β and time constant α to vary as shown in Figure 5. When α is fixed, and β is varied, we find dominance times decrease as depression strength increases in Figure 5(left). Thus, stronger depression leads to quicker switching between dominant populations, as one might expect. When β is fixed and α is varied, we find that dominance times decrease as the depression time constant is increased in Figure 5(right). This arises from the fact that the timescale of recovery from depression is set by α, but the timescale of depression activation is set by the parameter β.

3.2. Noise-generated oscillations. Recordings from the brain and reports by subjects during binocular rivalry tasks show dominance time statistics that may be fit to a gamma distribution [46]. In addition, statistical analysis of such data shows little correlation between one dominance time and the next [41, 42, 46]. This suggests that the switching between one eye's dominance and the next may be largely driven by a stochastic process. Some previous models have accounted for this by presuming that the input arriving at the network encoding

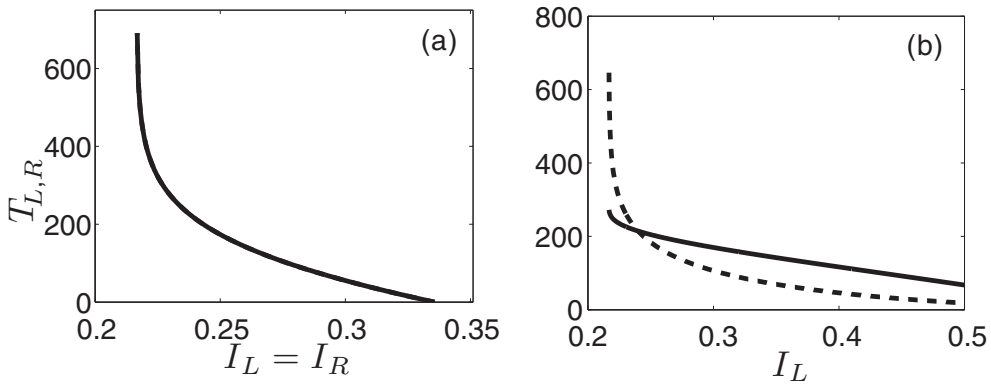

Figure 4. *Dominance times calculated from* (3.27) *and* (3.28) *plotted against input amplitude.* (a) *Effect of changing the amplitude of both inputs* $I_L = I_R = I$ *on the dominance times of both percepts. In this case, dominance times are identical.* (b) *Effect of changing input to left eye* (I_L) *on dominance times of left population* u_L *(dashed curve) and right population (solid curve) when* $I_R = 0.24$. *Other parameters are as in Figure* 3.

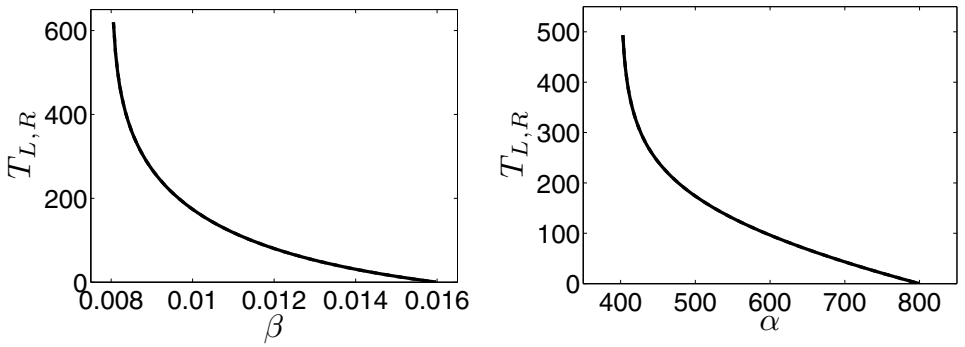

Figure 5. *Dominance times calculated from* (3.27) *and* (3.28) *plotted against (left) synaptic depression strength* β *and (right) time constant* α. *Parameter values are* $\kappa = 0.05$, $I_L = I_R = 0.25$, $\bar{w}_c = -1$, $\alpha = 500$, *and* $\beta = 0.01$ *unless otherwise stated.*

rivalry is stochastic, so the noise is extrinsic [41, 25]. Recent modeling efforts have examined and compared the effects of dominance switching due to an additive noise term in the activity variable of a firing rate model versus a deterministic slow-adapting variable [49, 52]. Laing and Chow's spiking neuron model of binocular rivalry contained no stochastic process, but statistics of resulting dominance times in the model appeared noisy due to the aperiodicity of the high-dimensional system's trajectories [39]. We follow up on firing rate studies with additive noise by comparing the effects of including a noise term in the activity variables of our system and the depression variable on dominance times.

To account for the random behavior in the model, we employ the following equation for independent input noise to each variable [52]:

$$\dot{n}_j(t) = -\frac{n_j(t)}{\nu} + \gamma\sqrt{2/\nu}\mu(t), \qquad j = L, R, \tag{3.29}$$

where $\mu(t)$ is white noise with zero mean and unit variance. Thus, the trajectory $n_j(t)$ will follow an Ornstein–Uhlenbeck process with standard deviation γ and timescale ν. We apply this noise to either the two activity variables $u_{L,R}$ or the two depression variables $q_{L,R}$. When we include this term as additive noise to only the activity variables, $u_{L,R}$, we replace each of their deterministic governing equations in (3.1) with

$$\dot{u}_j(t) = -u_j(t) + \bar{w}_l q_j(t)\Theta(u_j(t)-\kappa) + \bar{w}_c q_k(t)\Theta(u_k(t)-\kappa) + I_j(t) + n_j(t), \quad j = L, R \text{ and } j \neq k. \tag{3.30}$$

This mimics the input drive to both neural populations being noisy. In addition, we examine the effect of including an additive noise term in the depression variables, $q_{L,R}$, by employing the following equation for their dynamics in place of their original deterministic equation in (3.1):

$$\dot{q}_j(t) = (1-q_j(t))/\alpha - \beta q_j(t)\Theta(u_j(t)-\kappa) + n_j(t), \qquad j = L, R. \tag{3.31}$$

We also impose the conditions $q_j(t) \in [0,1]$ for all t and $j = L, R$, which ensures that each synaptic strength retains its proper sign and that the variables $q_j(t)$ cannot act to impose dynamic facilitation. To numerically simulate the stochastic system modified by either (3.30) or (3.31), we employ the Euler–Maruyama method.

We summarize the results of including additive noise in the deterministic system (3.1) by plotting distributions of dominance times along with the data series' autocorrelations. In parameter ranges where the deterministic version of the system would support only a WTA solution, we found that additive noise in either the activity or depression variables was sufficient to generate stochastic oscillations in the system. Following simulations of (3.1) along with either (3.30) or (3.31) for a sufficiently long period, we compute the lengths of time of all dominance durations. Population j is dominant if $u_j > u_k$ ($j \neq k$). The autocorrelation coefficient is then also calculated for this series of dominance times for various lags. In Figure 6 we compare the effects of additive noise on the activity versus the depression variables. When additive noise is included in activity variables $u_{L,R}$, we find that this can generate a peak in the dominance duration distribution at $T \approx 200$ (2 seconds) with a long tail at higher dominance times. However, there is a sharp peak in distributions near $T = 0$ as well. This arises from activity falling below threshold and then being kicked back above by additive noise prior to its relaxation to a suppressed state. We do not find this same behavior when additive noise is included in the depression variables $q_{L,R}$ (see Figure 6(right)). In fact, there is a peak in the dominance duration distribution at $T \approx 200$ and an even longer tail at higher dominance times. Yet, there is no peak in dominance times close to $T = 0$. This is perhaps due to additional temporal filtering occurring due to the longer time constant α of the depression variables. Thus, the distribution generated here could be more feasibly fit to a gamma distribution as in previous experimental and modeling studies of binocular rivalry [46, 39, 49, 52]. In Figure 7, we plot the autocorrelation statistics of the time series of dominance durations used to construct the histograms in Figure 6. We do find correlations for nonzero lag in dominance times of the network with noise in the activity variables. However, there is little to no correlation for nonzero lag in the dominance times of the network with noise in the depression variables. When the neural activity variables are noise driven, there is

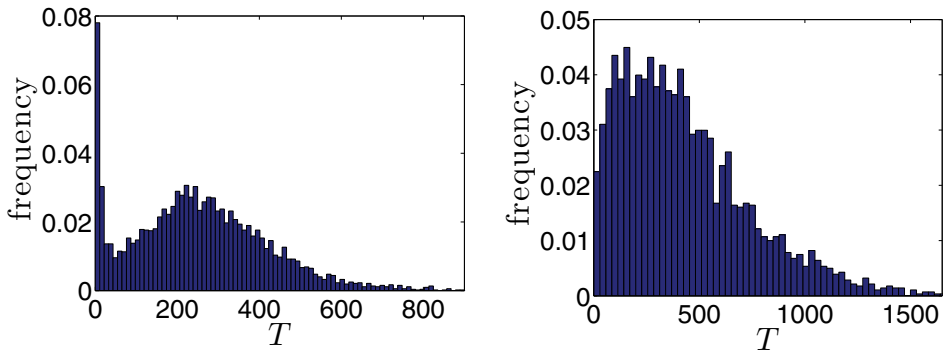

Figure 6. *Distribution of dominance durations for stochastic variations of the deterministic system* (3.1). *(Left) Additive noise is included in the activity variables* $u_{L,R}$ *by replacing the equations for them with* (3.30). *Exponentially filtered white noise has variance* $\gamma = 0.11$. *Note that the distribution has a peak around* $T = 200$. *(Right) Additive noise is included in the depression variables* $q_{L,R}$ *by replacing the equations for them with* (3.31). *Exponentially filtered white noise has variance* $\gamma = 0.01$. *In both panels, the system was simulated for* 5×10^6 *time units. Other parameters are* $\kappa = 0.05$, $\bar{w}_l = 0.04$, $\bar{w}_c = -1$, $\alpha = 500$, $\beta = 0.01$, *and* $\nu = 50$.

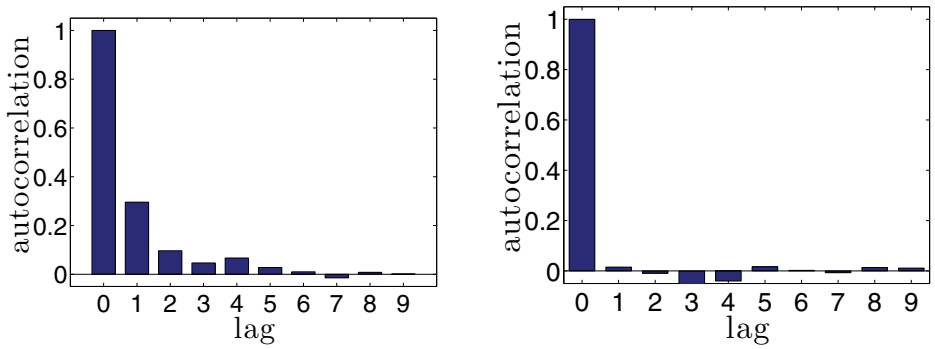

Figure 7. *Autocorrelations for the time series of dominance durations shown in Figure* 6 *when (left) noise is added to activity variables* $u_{L,R}$ *and (right) noise is added to depression variables* $q_{L,R}$.

still reliable memory in the system due to the presence of the wholly deterministic depression variables. The interplay between noise driven oscillations versus oscillations generated by slow adaptive variables in competitive neural networks is an ongoing area of research [41, 25, 49].

3.3. Equilibria of network with smooth sigmoid firing rate. One potential question regarding the study of system (3.1) with a Heaviside firing rate function regards just how representative are its dynamics of firing rate models with a smooth sigmoidal firing rate function (2.2). We probe this question now by using numerical methods to characterize the bifurcation structure of the network for finite gain η. A previous study in [52] of a similar competitive neural network with depression and a smooth sigmoid firing rate found that in addition to an off, WTA, fusion, and escape rivalry state, the network could support release rivalry for low levels of input. By release rivalry, we mean that oscillations are generated by a release mechanism where the dominant population falls below threshold prior to the

suppressed population rising above threshold (see Figure 8(left), for example). This generates dominance times in rivalry that increase as the strength of input is increased, which is in fact contrary to the general results of experimental recordings and psychophysical data of binocular rivalry [45, 9, 46]. In [52], the effect that the strength of inputs and depression had upon the stability of steady states was examined, but the effect of varying the strength of the gain of the firing rate function was not. To follow up on this previous study, we examine the role that the gain of the firing rate function has upon the dynamics of the competitive neural network with synaptic depression (3.1).

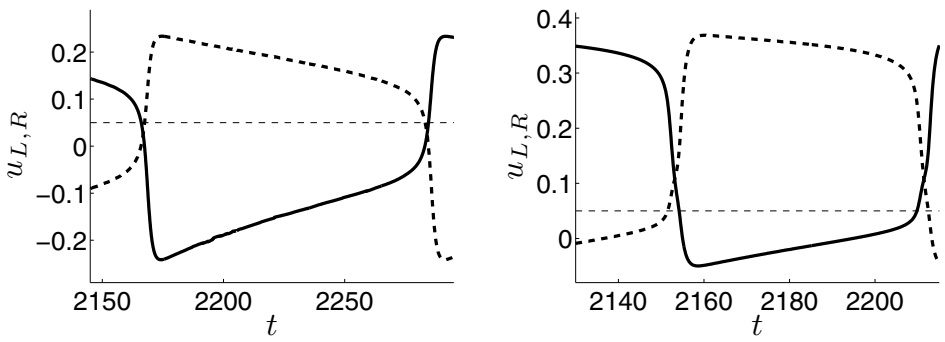

Figure 8. *Oscillatory solutions of the space-clamped system (3.1) for a smooth sigmoid activation function (2.2). (Left) Plot against time of the activities u_L (solid black) and u_R (dashed black) where switching during oscillations is induced by a release mechanism. Here, the strengths of the inputs are $I_L = I_R = 0.1$ and the gain of the sigmoid is $\eta = 15$. (Right) Plot against time of the activities u_L, u_R where switching during oscillations is induced by an escape mechanism. Here, the strengths of inputs are $I_L = I_R = 0.25$ and the gain of the sigmoid is $\eta = 65$. Other parameters are $\bar{w}_l = 0.4$, $\bar{w}_c = -1$, $\kappa = 0.05$, $\alpha = 500$, and $\beta = 0.01$. The horizontal dashed line represents the value of the threshold κ.*

First, we find that system (3.1) in the case of a smooth sigmoid firing rate function supports both a rivalry and escape mechanism for generating oscillations. In Figure 8(left), we plot a numerical simulation of the system (3.1), which occurs for sufficiently weak input and gain. Notice that the dominant population's activity falls below threshold prior to the suppressed population's rising above threshold. The opposite is true in Figure 8(right), where escape rivalrous oscillations are shown. This occurs for sufficiently large input and gain. Next, in Figure 9 we summarize the two possible bifurcation scenarios when gain η is the varied parameter. As shown in Figure 9(left), for weak input ($I_L = I_R = 0.1$), we find that when the gain is weak, only a stable off state exists. However, as the gain is increased, a limit cycle arises through a supercritical Hopf bifurcation, which is the onset of rivalry through a release mechanism. At sufficiently high gain ($\eta \approx 30$), the limit cycle vanishes and only a WTA solution exists. This behavior persists as $\eta \to \infty$. Therefore, for a sufficiently large gain, the behavior of system (3.1) with a smooth sigmoid firing rate (2.2) is quite similar to that when it has a Heaviside firing rate (2.3). In Figure 9(right), we show that for strong input, the system possesses only a fusion state for low gain, but at a critical higher gain ($\eta \approx 60$), we find that there is an escape rivalry/fusion bistable state, which is the same general structure the network has as $\eta \to \infty$. Thus, the bistable state is a generic behavior of system (3.1), so there must be a separatrix between the fusion and rivalry states.

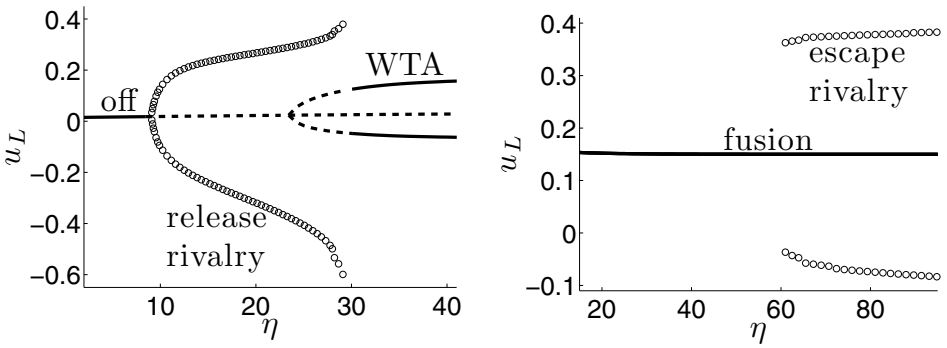

Figure 9. *Equilibria of the left population u_L as a function of the gain η of the smooth sigmoid activation function (2.2). Solid lines represent stable states, dashed lines represent unstable states, and circles represent maximum and minimum of rivalrous oscillations. (Left) For lower input $I_L = I_R = 0.1$ to both populations, increasing the gain leads to a destabilization of the off state through a supercritical Hopf bifurcation. The resultant limit cycle is generated through a release mechanism as shown in Figure 8(left). Eventually, this limit cycle vanishes for high gain ($\eta \approx 30$) and WTA equilibria remain as $\eta \to \infty$. (Right) For higher input to both populations $I_L = I_R = 0.25$ a fusion state exists for all levels of gain, but a limit cycle generated by an escape mechanism (see Figure 8(right)) arises for high gain ($\eta \approx 60$). This rivalry/fusion bistable state remains as $\eta \to \infty$. Other parameters are $\kappa = 0.05$, $\alpha = 500$, $\beta = 0.01$, $\bar{w}_l = 0.4$, and $\bar{w}_c = -1$.*

4. Oscillations in the coupled hypercolumn model. Let us now return to the full spatially extended coupled hypercolumn model (2.1). In a previous study, we showed that stable stationary bumps of activity can exist in a scalar neural field model with lateral inhibition for sufficiently weak synaptic depression [12, 37]. Additionally, it has been shown that a single ring (or hypercolumn) model with synaptic depression can support stable stationary bumps as well as a rotating bumps [69]. We extend these results here by considering two coupled rings (hypercolumns) with synaptic depression driven by stimuli with different orientations. A related study based on networks with spike frequency adaptation is considered elsewhere [47]. We consider the system (2.1) in the case of the Heaviside firing rate function (2.3) and inputs $I_L(\theta)$ and $I_R(\theta)$ given by functions peaked at a specific orientation, which are meant to represent stationary grating stimuli [6, 66]. For concreteness, we take

$$I_L(\theta) = I_L^0 \cos^p(\theta - \pi/4), \qquad I_R(\theta) = I_R^0 \cos^p(\theta + \pi/4), \tag{4.1}$$

where $\pi/4$ and $-\pi/4$ are the stimulus orientations and p is an even integer power that determines the sharpness of the inputs with respect to orientation. (We set $p = 6$.) The particular choice of stimulus orientations simplifies our calculations, since the associated neural field equations are reflection symmetric. That is, they are equivariant with respect to the transformation $L \to R$ and $\theta \to -\theta$. As a further simplification, we also take the left and right input strengths to be the same: $I_L^0 = I_R^0 = I_0$. Note, however, that our analysis can be extended to take into account more general stimulus orientations and asymmetric input strengths $I_L^0 \neq I_R^0$. Finally, we take both the local and cross-populations' weight functions w_l, w_c to be the harmonic weight function (2.4). Our analysis then proceeds by studying the existence and linear stability of nontrivial stationary solutions corresponding to either single bump or double bump solutions. A stationary solution $(u_L, u_R, q_L, q_R) = (U_L(\theta), U_R(\theta), Q_L(\theta), Q_R(\theta))$ of equations

(2.1) satisfies the system of equations (for $f(u) \equiv \Theta(u-\kappa)$)

$$\begin{aligned} U_L(\theta) &= w_l * (Q_L \Theta(U_L - \kappa)) + w_c * (Q_R \Theta(U_R - \kappa)) + I_L(\theta), \\ U_R(\theta) &= w_l * (Q_R \Theta(U_R - \kappa)) + w_c * (Q_L \Theta(U_L - \kappa)) + I_R(\theta), \\ Q_j(\theta) &= 1 - \frac{\alpha\beta\Theta(U_j(\theta)-\kappa)}{1+\alpha\beta\Theta(U_j(\theta)-\kappa)}, \quad j = L, R. \end{aligned} \tag{4.2}$$

Introduce the excited or superthreshold regions $R[U_j] = \{\theta | U_j(\theta) > \kappa\}$ of the left ($j = L$) and right ($j = R$) populations. These will vary depending on whether we study a single or double bump. A single bump solution is equivalent to a WTA scenario where only a single hypercolumn contains superthreshold bump activity—for example, $R[U_L] = (\theta_1, \theta_2)$ and $R[U_R] = \emptyset$. On the other hand, in the case of a double bump solution both hypercolumns exhibit superthreshold bump activity. Exploiting the reflection symmetry, this means that $R[U_L] = (\theta_1, \theta_2)$ and $R[U_R] = (-\theta_1, -\theta_2)$.

4.1. Existence of single bumps. For a single bump or WTA solution, only one neural activity variable will have an associated nonempty excited region, so we pick the left population such that $R[U_L] = (\theta_1, \theta_2)$, whereas the right population U_R will always remain below threshold so that $R[U_R] = \emptyset$. Threshold crossing points are then defined as $U_L(\theta_1) = U_L(\theta_2) = \kappa$. We could just as easily have picked the right population due to the reflection symmetry of the network. As we have prescribed, the system (4.2) becomes

$$U_L(\theta) = \int_{\theta_1}^{\theta_2} w_l(\theta - \theta') Q_L(\theta') \mathrm{d}\theta' + I_L(\theta), \tag{4.3}$$

$$U_R(\theta) = \int_{\theta_1}^{\theta_2} w_c(\theta - \theta') Q_L(\theta') \mathrm{d}\theta' + I_R(\theta), \tag{4.4}$$

$$Q_j(\theta) = 1 - \frac{\alpha\beta\Theta(U_j(\theta)-\kappa)}{1+\alpha\beta\Theta(U_j(\theta)-\kappa)}, \quad j = L, R. \tag{4.5}$$

Substituting (4.5) into (4.3) and (4.4) yields

$$U_L(\theta) = \frac{1}{1+\alpha\beta} \int_{\theta_1}^{\theta_2} w_l(\theta - \theta') \mathrm{d}\theta' + I_L(\theta), \tag{4.6}$$

$$U_R(\theta) = \frac{1}{1+\alpha\beta} \int_{\theta_1}^{\theta_2} w_c(\theta - \theta') \mathrm{d}\theta' + I_R(\theta). \tag{4.7}$$

Plugging in the sum of harmonics weight function (2.4) for w_l and w_c, we analytically calculate the single bump solution

$$U_L(\theta) = \frac{1}{1+\alpha\beta} \left[w_0^l(\theta_2 - \theta_1) + \frac{w_2^l}{2} (\sin(2(\theta - \theta_1)) - \sin(2(\theta - \theta_2))) \right] + I_L(\theta), \tag{4.8}$$

$$U_R(\theta) = \frac{1}{1+\alpha\beta} \left[w_0^c(\theta_2 - \theta_1) + \frac{w_2^c}{2} (\sin(2(\theta - \theta_1)) - \sin(2(\theta - \theta_2))) \right] + I_R(\theta). \tag{4.9}$$

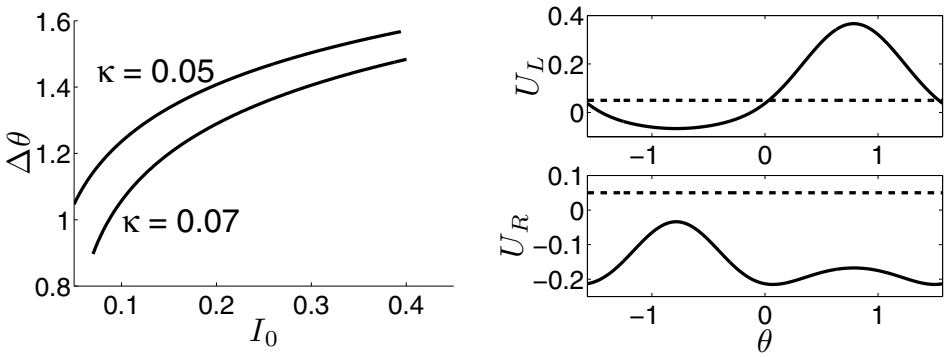

Figure 10. *Single bumps in coupled hypercolumns. (Left) Plots relating single bump width $\Delta\theta$ to the amplitude of input I_0 for different values of κ using (4.10) and constrained by inequality (4.12). For sufficiently large inputs I_0 and fixed threshold κ bumps do not exist, since the subthreshold condition (4.12) is no longer satisfied. Other parameters are $w_0^l = 0$, $w_2^l = 0.4$, $w_0^c = -1$, $w_2^c = 0.5$, $\alpha = 500$, and $\beta = 0.01$. (Right) Bump profile when $\kappa = 0.05$ and $I_0 = 0.3$.*

Applying the threshold conditions $U_L(\theta_1) = U_L(\theta_2) = \kappa$ and noting the reflection symmetry of the system, we have

$$\kappa = \frac{1}{1+\alpha\beta}\left[w_0^l \Delta\theta + \frac{w_2^l}{2}\sin(2\Delta\theta)\right] + I_0 \cos^p(\Delta\theta/2), \tag{4.10}$$

which provides us with an implicit equation relating the bump width $\Delta\theta = \theta_2 - \theta_1$ to all other parameters. Note that we have used the fact that the threshold crossing points are symmetric about $\pi/4$; that is, $\theta_1 = \pi/4 - \Delta\theta/2$ and $\theta_2 = \pi/4 + \Delta\theta/2$. One additional constraint on the solution (4.9) is that it always remains below threshold. For sufficiently strong inputs, the maximum of U_R will occur at the peak of the input I_R so that we need only check if $U_R(-\pi/4) < \kappa$, which we compute as

$$\begin{aligned} U_R(-\pi/4) &= \frac{1}{1+\alpha\beta}\left[w_0^c(\Delta\theta) + \frac{w_2^c}{2}(\sin(2\theta_2 + \pi/2) - \sin(2\theta_1 + \pi/2))\right] + I_0 \\ &= \frac{1}{1+\alpha\beta}\left[w_0^c(\Delta\theta) - w_2^c \sin(\Delta\theta)\right] + I_0. \end{aligned} \tag{4.11}$$

This yields

$$w_0^c(\Delta\theta) - w_2^c \sin(\Delta\theta) < (1+\alpha\beta)(\kappa - I_0) \tag{4.12}$$

for the subthreshold condition. Thus, for a single bump solution to exist, the threshold condition (4.10) and the subthreshold condition (4.12) must be satisfied. Equation (4.10) can be solved numerically using a root finding algorithm. Following this, we can find whether the inequality (4.12) is satisfied by direct computation. The variation of the width of the bump $\Delta\theta$ with the input strength I_0 and depression strength β is shown in Figure 10; the stability of the bump is calculated below.

4.2. Stability of single bumps. To study the stability of the single bump solution, we cannot use the technique of Taylor expanding equations (2.1) about a bump solution in the case of a smooth sigmoid firing rate (2.2) and then taking the high-gain limit of the associated Evans function [18]. This is due to a result we have recently shown [37], which is that the size of perturbation in which the Evans function approach is valid becomes vanishingly small in the high-gain limit. Thus, even in a version of system (2.1) with a steep but smooth firing rate function, stability results obtained for bumps using linear theory that employs an Evans function approach will be valid in a tiny region of phase space. Therefore, we utilize a more careful treatment of local stability that considers the fact that system (2.1) is piecewise-smooth [37, 12]. It should be stated up front that this approach can characterize only the stability of perturbations with real eigenvalues, which allows us to state sufficient conditions for instability. In practice, we find this characterizes the dynamics evolving from a perturbed standing bump solution quite well (see numerical results in section 5).

We begin by letting $u_j(\theta,t) = U_j(\theta)+\varepsilon\psi_j(\theta,t)$ and $q_j(\theta,t) = Q_j(\theta)+\varepsilon\varphi_j(\theta,t)$ for $j = L, R$, where ψ_j and φ_j denote smooth perturbations and $\varepsilon \ll 1$. Substituting this into the full system (2.1), imposing the single bump solutions (4.3), (4.4), and (4.5), and dividing through by ε gives

$$\begin{aligned}\frac{\partial\psi_L(\theta,t)}{\partial t} &= -\psi_L(\theta,t) + \frac{1}{\varepsilon}w_l * (Q_L[\Theta(U_L+\varepsilon\psi_L-\kappa)-\Theta(U_L-\kappa)])\\ &\quad + w_l * (\varphi_L\Theta(U_L+\varepsilon\psi_L-\kappa)),\end{aligned} \tag{4.13}$$

$$\begin{aligned}\frac{\partial\psi_R(\theta,t)}{\partial t} &= -\psi_R(\theta,t) + \frac{1}{\varepsilon}w_c * (Q_L[\Theta(U_L+\varepsilon\psi_L-\kappa)-\Theta(U_L-\kappa)])\\ &\quad + w_c * (\varphi_L\Theta(U_L+\varepsilon\psi_L-\kappa)),\end{aligned} \tag{4.14}$$

$$\begin{aligned}\frac{\partial\varphi_j(\theta,t)}{\partial t} &= -\frac{\varphi_j(\theta,t)}{\alpha} - \frac{\beta}{\varepsilon}Q_j[\Theta(U_j+\varepsilon\psi_j-\kappa)-\Theta(U_j-\kappa)]\\ &\quad - \beta\varphi_j\Theta(U_j+\varepsilon\psi_j-\kappa)\end{aligned} \tag{4.15}$$

for $j = L, R$. Denote the perturbations of the bump boundaries by $\varepsilon\Delta_{\pm}^L(t)$ such that

$$u_L(\theta_1+\varepsilon\Delta_-^L(t),t) = u_L(\theta_2+\varepsilon\Delta_+^L(t),t) = \kappa. \tag{4.16}$$

Taylor expanding these threshold conditions to first order in ε, we find that

$$\Delta_-^L(t) \approx -\frac{\psi_L(\theta_1,t)}{|U_L'(\theta_1)|}, \quad \Delta_+^L(t) \approx \frac{\psi_L(\theta_2,t)}{|U_L'(\theta_2)|}. \tag{4.17}$$

Following [12, 37], we can smooth out discontinuities in (4.15) by introducing the infinitesimal fields

$$\Phi_{Lm}(\theta,t) = \int_{\theta_1+\varepsilon\Delta_-^L}^{\theta_2+\varepsilon\Delta_+^L} w_m(\theta-\theta')\varphi_L(\theta',t)\mathrm{d}\theta' \tag{4.18}$$

for $m = l, c$. Therefore, even though $\mathcal{O}(1/\varepsilon)$ pointwise changes in $\varphi_L(x,t)$ may occur, the bump solution may still be stable, as the region over which $\mathcal{O}(1/\varepsilon)$ changes occur may shrink

to zero. This possibility is accounted for, since the dynamics of the field $\Phi_{Lm}(x,t)$ $(m=l,c)$ will remain $\mathcal{O}(1)$ when $\varphi_L(x,t)$ is $\mathcal{O}(1/\varepsilon)$ over an infinitesimal interval.

If we now differentiate (4.18) with respect to time, we find

$$\begin{aligned}(4.19)\quad \frac{\partial \Phi_{Lm}(\theta,t)}{\partial t} &= \int_{\theta_1+\varepsilon\Delta_-^L}^{\theta_2+\varepsilon\Delta_+^L} w_m(\theta-\theta')\frac{\partial \varphi_L(\theta',t)}{\partial t}\mathrm{d}\theta' \\ &\quad + \varepsilon w_m(\theta-\theta_2-\varepsilon\Delta_+^L(t))\varphi_L(\theta_2+\varepsilon\Delta_+^L(t),t)\dot{\Delta}_+^L(t) \\ &\quad - \varepsilon w_m(\theta-\theta_1-\varepsilon\Delta_-^L(t))\varphi_L(\theta_1+\varepsilon\Delta_-^L(t),t)\dot{\Delta}_-^L(t), \qquad m=l,c,\end{aligned}$$

where $\dot{\Delta}_\pm^L = \mathrm{d}\Delta_\pm^L/\mathrm{d}t$. We can now substitute (4.15) for $\partial\varphi_L/\partial t$. Note that the final term in (4.15) involves a Heaviside function, which will be nonzero only when the stationary bump U_L plus the perturbation $\varepsilon\psi_L$ is greater than the threshold κ. This region is precisely defined by the interval $(\theta_1+\varepsilon\Delta_-^L, \theta_2+\varepsilon\Delta_+^L)$, over which the integral in (4.19) is taken. This implies that the resulting term

$$\int_{\theta_1+\varepsilon\Delta_-^L}^{\theta_2+\varepsilon\Delta_+^L} w_m(\theta-\theta')\varphi_L(\theta',t)\Theta(U_L(\theta',t)+\varepsilon\psi_L(\theta',t)-\kappa)\mathrm{d}\theta' = \Phi_{Lm}(\theta,t).$$

Therefore, by modifying (4.13), (4.14), and (4.15) with the auxiliary variable definition given in (4.18) we have the alternative system of equations

$$\begin{aligned}(4.20)\quad \frac{\partial \psi_L(\theta,t)}{\partial t} &= -\psi_L(\theta,t)+\Phi_{Ll}(\theta,t) \\ &\quad + \frac{1}{\varepsilon}\int_{\theta_1+\varepsilon\Delta_-^L(t)}^{\theta_2+\varepsilon\Delta_+^L(t)} w_l(\theta-\theta')Q_L(\theta')\mathrm{d}\theta' - \frac{1}{\varepsilon}\int_{\theta_1}^{\theta_2} w_l(\theta-\theta')Q_L(\theta')\mathrm{d}\theta',\end{aligned}$$

$$\begin{aligned}(4.21)\quad \frac{\partial \psi_R(\theta,t)}{\partial t} &= -\psi_R(\theta,t)+\Phi_{Lc}(\theta,t) \\ &\quad + \frac{1}{\varepsilon}\int_{\theta_1+\varepsilon\Delta_-^L(t)}^{\theta_2+\varepsilon\Delta_+^L(t)} w_c(\theta-\theta')Q_L(\theta')\mathrm{d}\theta' - \frac{1}{\varepsilon}\int_{\theta_1}^{\theta_2} w_c(\theta-\theta')Q_L(\theta')\mathrm{d}\theta',\end{aligned}$$

$$\begin{aligned}(4.22)\quad \frac{\partial \Phi_{Lm}(\theta,t)}{\partial t} &= -(\alpha^{-1}+\beta)\Phi_{Lm}(\theta,t) \\ &\quad - \frac{\beta}{\varepsilon}\int_{\theta_1+\varepsilon\Delta_-^L(t)}^{\theta_2+\varepsilon\Delta_+^L(t)} w_m(\theta-\theta')Q_L(\theta')[\Theta(U_L+\varepsilon\psi_L-\kappa)-\Theta(U_L-\kappa)]\mathrm{d}\theta \\ &\quad + \varepsilon w_m(\theta-\theta_2-\varepsilon\Delta_+^L(t))\varphi_L(\theta_2+\varepsilon\Delta_+^L(t),t)\dot{\Delta}_+^L(t) \\ &\quad - \varepsilon w_m(\theta-\theta_1-\varepsilon\Delta_-^L(t))\varphi_L(\theta_1+\varepsilon\Delta_-^L(t),t)\dot{\Delta}_-^L(t), \qquad m=l,c.\end{aligned}$$

We can now linearize the system of equations (4.20), (4.21), and (4.22) by expanding in powers of ε and collecting all $\mathcal{O}(1)$ terms. Note that it is important to keep track of the signs of $\Delta_\pm^L$

when approximating the various integrals due to the discontinuous nature of $Q_L(\theta)$. We thus obtain the pseudolinear system of equations

$$\begin{aligned}\frac{\partial \psi_L(\theta,t)}{\partial t} &= -\psi_L(\theta,t)+\Phi_{Ll}(\theta,t)+\gamma_S w_l(\theta-\theta_1)\psi_L(\theta_1,t)G(\psi_L(\theta_1,t))\\ &\quad +\gamma_S w_l(\theta-\theta_2)\psi_L(\theta_2,t)G(\psi_L(\theta_2,t)),\end{aligned} \tag{4.23}$$

$$\begin{aligned}\frac{\partial \psi_R(\theta,t)}{\partial t} &= -\psi_R(\theta,t)+\Phi_{Lc}(\theta,t)+\gamma_S w_c(\theta-\theta_1)\psi_L(\theta_1,t)G(\psi_L(\theta_1,t))\\ &\quad +\gamma_S w_c(\theta-\theta_2)\psi_L(\theta_2,t)G(\psi_L(\theta_2,t)),\end{aligned} \tag{4.24}$$

$$\begin{aligned}\frac{\partial \Phi_{Lm}(\theta,t)}{\partial t} &= -(\alpha^{-1}+\beta)\Phi_{Lm}(\theta,t)\\ &\quad -\beta(\gamma_S w_m(\theta-\theta_1)\psi_L(\theta_1,t)G(\psi_L(\theta_1,t))\Theta(\psi_L(\theta_1,t))\\ &\quad +\gamma_S w_m(\theta-\theta_2)\psi_L(\theta_2,t)G(\psi_L(\theta_2,t))\Theta(\psi_L(\theta_2,t))), \qquad m=l,c,\end{aligned} \tag{4.25}$$

where G is the step function

$$G(\Delta)=\begin{cases}1 & \text{if } \Delta>0,\\ (1+\alpha\beta)^{-1} & \text{if } \Delta<0,\end{cases} \tag{4.26}$$

and

$$(\gamma_S)^{-1}=|U_L'(\theta_k)|=\left|\frac{1}{1+\alpha\beta}\Big[w_l(\theta_k-\theta_1)-w_l(\theta_k-\theta_2)\Big]+I_L'(\theta_k)\right| \tag{4.27}$$

for $k=1,2$.

Equations (4.23)–(4.25) imply that the local stability of the stationary bump solution depends upon the spectral properties of a pseudolinear operator. In a previous study, we solved a similar problem by assuming that solutions were nonoscillatory, which generated a simpler spectral problem dependent on the sign of perturbations [12]. Here, we make a similar assumption, namely, that the perturbations $\psi_L(\theta_1,t)$ and $\psi_L(\theta_2,t)$ (equivalently Δ_-^L and Δ_+^L) do not switch signs. In other words, we assume that (4.23)–(4.25) have separable solutions of the form $(\psi_L(\theta,t),\psi_R(\theta,t),\Phi_{Ll}(\theta,t),\Phi_{Lc}(\theta,t))=\mathrm{e}^{\lambda t}(\psi_L(\theta),\psi_R(\theta),\Phi_{Ll}(\theta),\Phi_{Lc}(\theta))$, where λ is real.[2] The step functions Θ, G are then time-independent, so there is a common factor $\mathrm{e}^{\lambda t}$ that cancels everywhere. We thus obtain an eigenvalue problem of the form

$$\begin{aligned}(\lambda+1)\psi_L(\theta) &= \gamma_S w_l(\theta-\theta_1)\psi_L(\theta_1)G(\psi_L(\theta_1))\left(1-\frac{\beta\Theta(\psi_L(\theta_1))}{\lambda+\alpha^{-1}+\beta}\right)\\ &\quad +\gamma_S w_l(\theta-\theta_2)\psi_L(\theta_2)G(\psi_L(\theta_2))\left(1-\frac{\beta\Theta(\psi_L(\theta_2))}{\lambda+\alpha^{-1}+\beta}\right),\end{aligned} \tag{4.28}$$

$$\begin{aligned}(\lambda+1)\psi_R(\theta) &= \gamma_S w_c(\theta-\theta_1)\psi_L(\theta_1)G(\psi_L(\theta_1))\left(1-\frac{\beta\Theta(\psi_L(\theta_1))}{\lambda+\alpha^{-1}+\beta}\right)\\ &\quad +\gamma_S w_c(\theta-\theta_2)\psi_L(\theta_2)G(\psi_L(\theta_2))\left(1-\frac{\beta\Theta(\psi_L(\theta_2))}{\lambda+\alpha^{-1}+\beta}\right).\end{aligned} \tag{4.29}$$

[2]Restricting our stability analysis to real λ means that we can derive only sufficient conditions for the instability rather than stability of a single or double bump solution. Moreover, we cannot establish the existence of limit cycle oscillations in terms of standard Hopf bifurcation theory. Nevertheless, numerical simulations will establish that destabilization of a (double) bump solution can lead to oscillatory solutions suggestive of binocular rivalry; see section 5.

Note that we have assumed that $\lambda \neq -(\alpha^{-1}+\beta)$ so that we can use (4.25) to solve for $\Phi_{Ll}(\theta)$ and $\Phi_{Lc}(\theta)$ in terms of $\psi_L(\theta_1)$ and $\psi_L(\theta_2)$; the case $\lambda = -(\alpha^{-1}+\beta)$ does not contribute to any instabilities.

It is possible to show that the solutions for λ can be identified with the spectra of a set of compact linear operators acting in the space of bounded continuous functions on the interval $[\theta_1, \theta_2]$, along the lines of Guo and Chow [27, 12]. However, here we will simply calculate λ directly from the set of equations (4.28) and (4.29). In one class of solutions, we need only restrict the function $\psi_L(\theta)$ to vanish on the boundary, $\psi_L(\theta_1) = \psi_L(\theta_2) = 0$, so that $\psi_R(\theta)$ is unrestricted and $\lambda = -1$. This belongs to the essential spectrum, since $\lambda = -1$ has infinite multiplicity and does not contribute to any instabilities. The discrete spectrum is then obtained by setting $\theta = \theta_1$ and $\theta = \theta_2$ in (4.28), which determines both the eigenvalues λ and the pair $\psi_L(\theta_1), \psi_L(\theta_2)$ (up to a scale factor). Once these are known, the eigensolutions $\psi_L(\theta)$ and $\psi_R(\theta)$ on $\theta \in [-\pi/2, \pi/2)$ are fully determined by (4.28) and (4.29). Note that the resulting eigenvalue equation is qualitatively similar to one derived in the linearization of a single bump in a single network with synaptic depression [12, 37]. One major difference here is that the input to the network is inhomogeneous so that translation invariance is lost. Hence, we no longer expect a zero eigenvalue associated with uniform shifts. We distinguish four classes of eigensolution to (4.28) and (4.29): (i) $\psi_L(\theta_1) > 0$ and $\psi_L(\theta_2) < 0$; (ii) $\psi_L(\theta_1) < 0$ and $\psi_L(\theta_2) > 0$; (iii) $\psi_L(\theta_1) > 0$ and $\psi_L(\theta_2) > 0$; (iv) $\psi_L(\theta_1) < 0$ and $\psi_L(\theta_2) < 0$. The four types of perturbation correspond, respectively, to a leftward shift, a rightward shift, an expansion, and a contraction of the bump in the left eye hypercolumn. As the eigenvalue problem is qualitatively similar to our previous work, we merely summarize the stability properties for each class of perturbation.

(i) $\psi_L(\theta_1) > 0; \psi_L(\theta_2) < 0$. As has been shown in the spatially extended network with synaptic depression and no input, increasing the strength of synaptic depression β will lead to a destabilization of standing bumps through the shift perturbation. In fact, in all parameter regimes we have studied, this is the particular perturbation that destabilizes first.[3] In the case of a stimulus driven system, we find that inputs serve to move the onset of destabilization to a higher value of β. As before, we can study stability merely on the bump boundaries by setting $\theta = \theta_1, \theta_2$, which, along with our perturbation sign assumptions, yields

$$\begin{pmatrix} \Gamma_\beta(\lambda) - \gamma_S w_l(0)\left(\lambda + \alpha^{-1}\right) & -\gamma_S\left(\lambda + \alpha^{-1}\right) w_l(\Delta\theta) \\ -\gamma_S\left(\lambda + \alpha^{-1}\right) w_l(\Delta\theta) & \Gamma_\beta(\lambda) - \gamma_S w_l(0)\left(\lambda + \alpha^{-1}\right) \end{pmatrix} \begin{pmatrix} \psi_L(\theta_1) \\ \psi(\theta_2) \end{pmatrix}$$

$$= -\frac{\gamma_S \alpha\beta\lambda}{1+\alpha\beta} \begin{pmatrix} w_l(\Delta\theta)\psi_L(\theta_2) \\ w_l(0)\psi_L(\theta_2) \end{pmatrix}. \tag{4.30}$$

As in the case without inputs, we assume $\beta \ll 1$ and carry out a perturbation expansion in β. First, setting $\beta = 0$ in (4.30) shows that the lowest order solution is $\psi_0^- = -\psi_0^+$ with $\lambda_0 = -\alpha^{-1}$ as a degenerate eigenvalue and $\lambda_0 = -1 + \gamma_S(w_l(0) - w_l(\Delta\theta))$, which will always be negative, since $\gamma_S^{-1} > w_l(0) - w_l(\Delta\theta)$. All eigensolutions pick up $\mathcal{O}(\beta)$ corrections as β is

[3] More precisely, shift perturbations are the dominant instability associated with real eigenvalues. Our analysis cannot determine possible instabilities associated with complex eigenvalues. However, numerical simulations suggest that single bump solutions are stable for sufficiently small β and destabilize at the point where an eigenvalue associated with shift perturbations crosses the origin; see section 5.

then increased from zero, but we will show that the valid eigenvalue originating from $-\alpha^{-1}$ eventually becomes positive, signifying traveling pulse solutions. See [69] for a recent study of traveling pulse solutions in a ring model with synaptic depression.

(ii) $\psi_L(\theta_1) < 0; \psi_L(\theta_2) > 0$. Due to reflection symmetry of the original system, when w_l is an even function, the spectrum of rightward shifts is identical to that of leftward shifts.

(iii) $\psi_L(\theta_1) > 0; \psi_L(\theta_2) > 0$. In this case, if we set $\theta = \theta_1, \theta_2$, we have $\psi_L(\theta_1) = \psi_L(\theta_2) > 0$, so (4.28) and (4.29) become

$$(\lambda + \alpha^{-1} + \beta)(\lambda + 1) = (\lambda + \alpha^{-1})(1 + \alpha\beta)\Omega_I, \tag{4.31}$$

where

$$\Omega_I = \frac{w_l(0) + w_l(\Delta\theta)}{w_l(0) - w_l(\Delta\theta) + (1 + \alpha\beta)I_L'(\theta_1)} \tag{4.32}$$

and we have substituted for γ_S using (4.27). It then follows that $\lambda = \lambda_\pm$ with

$$\begin{aligned}\lambda_\pm = &\frac{1}{2}\left[\Omega_I(1 + \alpha\beta) - \left(1 + \alpha^{-1} + \beta\right)\right] \\ &\pm \frac{1}{2}\sqrt{\left[\Omega_I(1 + \alpha\beta) - (1 + \alpha^{-1} + \beta)\right]^2 + 4(\Omega_I - 1)\left(\alpha^{-1} + \beta\right)}.\end{aligned} \tag{4.33}$$

The associated eigenmode corresponds to a pure expansion of the bump.

(iv) $\psi_L(\theta_1) < 0; \psi_L(\theta_2) < 0$. In this final case, if we set $\theta = \theta_1, \theta_2$ and note that $\psi_L(\theta_1) = \psi_L(\theta_2)$, then (4.28) and (4.29) imply $\lambda = \lambda_0$ with

$$\lambda_0 = \Omega_I - 1. \tag{4.34}$$

The associated eigenmode corresponds to a pure contraction of the bump.

We illustrate the above analysis by considering stationary single bumps in the coupled hypercolumn network with a harmonic weight function (2.4). In particular, we plot eigenvalues for the destabilizing perturbations for the stimulus driven bump, which is stable as $\beta \to 0$. In Figure 11, we plot the maximal real eigenvalue associated with the shift perturbation (cases (i) and (ii)) as a function of β and as a function of I_0. The bump destabilizes to shift perturbations for sufficiently strong depression β. However, large inputs I_0 can keep the bump stable for larger values of β. In Figure 12, we plot the eigenvalues of the expansion and contraction perturbations as a function of β and I_0. In the case of contractions, there is a single negative branch of eigenvalues. In the case of expansions, there are two negative branches for fixed I_0 and sufficiently small β, which annihilate at the left edge of a forbidden region in which eigenvalues given by (4.33) are complex so that stability cannot be determined. At the other end of the forbidden region, a pair of positive branches emerges for sufficiently large β. By fixing β and varying I_0, we see that eigenvalues are slightly less sensitive to the input strength and remain the same sign over a wide range. We find that the lower branch of the expansion mode and the branch of the contraction mode never meet, as opposed to our previous study of a network without inhomogeneous input [12, 37].

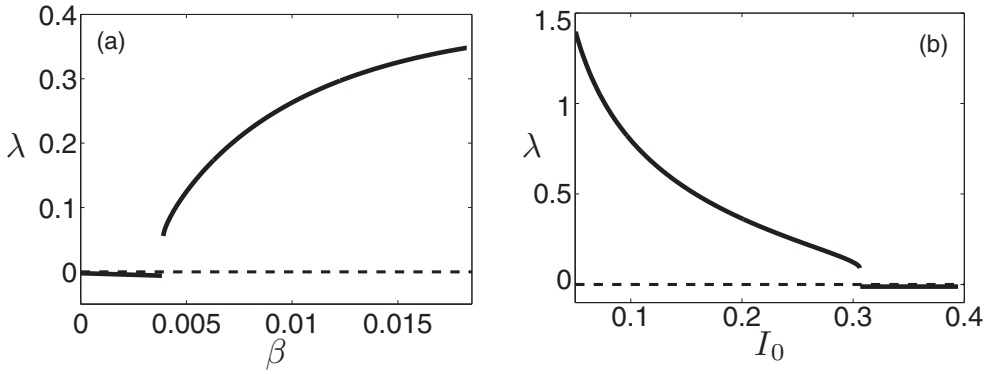

Figure 11. *Eigenvalues associated with shift perturbations of single bump (cases* (i) *and* (ii)*).* (a) *Maximal nonzero real eigenvalues plotted as a function of* β *for* $I_0 = 0.24$*. Bump is unstable with respect to shifts for sufficiently large* β*.* (b) *Maximal nonzero real eigenvalue plotted as a function of* I_0 *for* $\beta = 0.01$*. Bump is unstable with respect to shifts for sufficiently weak input* I_0*. Other parameters are* $\kappa = 0.05$*,* $w_0^l = 0$*,* $w_2^l = 0.4$*,* $w_0^c = -1$*,* $w_2^c = 0.5$*, and* $\alpha = 500$*.*

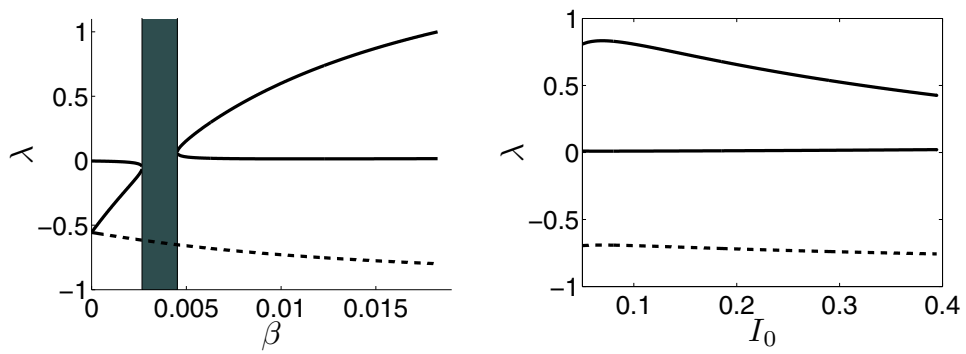

Figure 12. *Eigenvalues associated with expansion and contraction perturbations (cases* (iii) *and* (iv)*). (Left) Eigenvalues of the expansion (solid) and contraction (dashed) perturbations as a function of* β *when* $I_0 = 0.24$*. In the grey regions, the roots of* (4.33) *are complex, violating the ansatz that* λ *is real. (Right) Eigenvalues of the expansion (solid) and contraction (dashed) perturbations as a function of* I_0 *for* $\beta = 0.01$*. Other parameters are* $\kappa = 0.05$*,* $w_0^l = 0$*,* $w_2^l = 0.4$*,* $w_0^c = -1$*,* $w_2^c = 0.5$*, and* $\alpha = 500$*.*

4.3. Existence of double bump. For a double bump or fusion solution, neural activity variables will both have associated nonempty excited regions $R[U_L] = (\theta_1, \theta_2)$ and $R[U_R] = (-\theta_2, -\theta_1)$ and thus threshold crossing points $U_L(\theta_1) = U_L(\theta_2) = \kappa$ and $U_R(-\theta_2) = U_R(-\theta_1) = \kappa$. Therefore, by prescribing the double bump solution in both populations, equations (4.2) become

$$U_L(\theta) = \int_{\theta_1}^{\theta_2} w_l(\theta - \theta')Q_L(\theta')\mathrm{d}\theta' + \int_{-\theta_2}^{-\theta_1} w_c(\theta - \theta')Q_R(\theta')\mathrm{d}\theta' + I_L(\theta), \tag{4.35}$$

$$U_R(\theta) = \int_{-\theta_2}^{-\theta_1} w_l(\theta - \theta')Q_R(\theta')\mathrm{d}\theta' + \int_{\theta_1}^{\theta_2} w_c(\theta - \theta')Q_L(\theta')\mathrm{d}\theta' + I_R(\theta), \tag{4.36}$$

$$Q_j(\theta) = 1 - \frac{\alpha\beta\Theta(U_j(\theta) - \kappa)}{1 + \alpha\beta\Theta(U_j(\theta) - \kappa)}, \quad j = L, R. \tag{4.37}$$

Substituting (4.37) into (4.35) and (4.36) yields

$$U_L(\theta) = \frac{1}{1+\alpha\beta}\left[\int_{\theta_1}^{\theta_2} w_l(\theta-\theta')\mathrm{d}\theta' + \int_{-\theta_2}^{-\theta_1} w_c(\theta-\theta')\mathrm{d}\theta'\right] + I_L(\theta), \tag{4.38}$$

$$U_R(\theta) = \frac{1}{1+\alpha\beta}\left[\int_{-\theta_2}^{-\theta_1} w_l(\theta-\theta')\mathrm{d}\theta' + \int_{\theta_1}^{\theta_2} w_c(\theta-\theta')\mathrm{d}\theta'\right] + I_R(\theta). \tag{4.39}$$

Employing the sum of harmonics weight function (2.4), we can analytically calculate the double bump solutions

$$\begin{aligned} U_L(\theta) = \frac{1}{1+\alpha\beta}\Bigg[&(w_0^l + w_0^c)(\theta_2-\theta_1) + \frac{w_2^l}{2}(\sin(2(\theta-\theta_1)) - \sin(2(\theta-\theta_2))) \\ &+ \frac{w_2^c}{2}(\sin(2(\theta+\theta_2)) - \sin(2(\theta+\theta_1)))\Bigg] + I_L(\theta), \end{aligned} \tag{4.40}$$

$$\begin{aligned} U_R(\theta) = \frac{1}{1+\alpha\beta}\Bigg[&(w_0^l + w_0^c)(\theta_2-\theta_1) + \frac{w_2^l}{2}(\sin(2(\theta+\theta_2)) - \sin(2(\theta+\theta_1))) \\ &+ \frac{w_2^c}{2}(\sin(2(\theta-\theta_1)) - \sin(2(\theta-\theta_2)))\Bigg] + I_R(\theta). \end{aligned} \tag{4.41}$$

Applying the threshold conditions, we have

$$\begin{aligned} \kappa = \frac{1}{1+\alpha\beta}\Bigg[&(w_0^l + w_0^c)(\Delta\theta) + \frac{w_2^l}{2}\sin(2(\Delta\theta)) + \frac{w_2^c}{2}(\sin(2(\theta_2+\theta_1)) - \sin(4\theta_1))\Bigg] \\ &+ I_0\cos^p(\Delta\theta/2), \end{aligned} \tag{4.42}$$

$$\begin{aligned} \kappa = \frac{1}{1+\alpha\beta}\Bigg[&(w_0^l + w_0^c)(\Delta\theta) + \frac{w_2^l}{2}\sin(2(\Delta\theta)) + \frac{w_2^c}{2}(\sin(4\theta_2) - \sin(2(\theta_2+\theta_1)))\Bigg] \\ &+ I_0\cos^p(\Delta\theta/2), \end{aligned} \tag{4.43}$$

where $\Delta\theta = \theta_2 - \theta_1$, the width of each bump. Therefore, we have a system of implicit expressions that relate the threshold crossing points θ_1, θ_2 to all other parameters. The system prescribed by (4.42) and (4.43) can be solved numerically using a root finding algorithm. The variation of the width of each bump $\Delta\theta$ with the input strength I_0 is shown in Figure 13; the stability of these bumps is calculated below.

4.4. Stability of the double bump. As in section 4.2, we cannot calculate the stability of the double bump here using a standard Evans function approach, and we must account for the piecewise smooth nature of the dynamics more carefully. One caveat of this analysis is that we may only calculate the form of perturbations to the bump with a real eigenvalue characterizing their temporal evolution. While this may appear to be a barrier to calculating the stability boundary, the particular perturbation that leads to the oscillatory instability leading to rivalry, we are in fact able to characterize this boundary quite well with perturbations possessing real eigenvalues. We explain this issue further below as well as show examples of instabilities in section 5.

Due to the similarity our stability analysis of the double bump has to that of the single bump, we relegate this calculation to the appendix. After changing variables and accounting

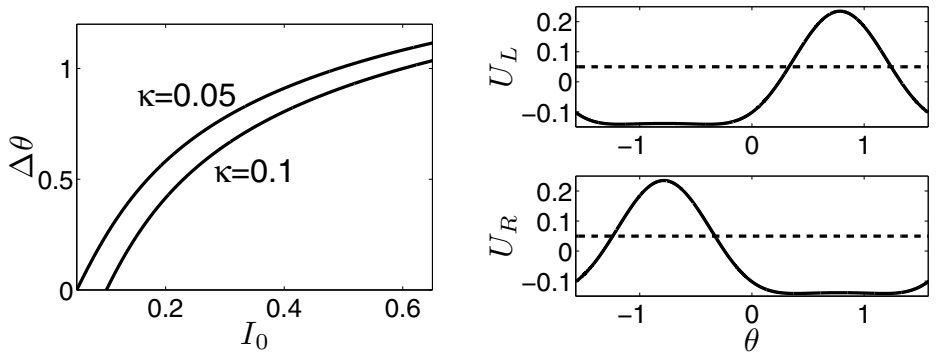

Figure 13. *Double bumps in coupled hypercolumns. (Left) Plots relating bump width $\Delta\theta$ to the amplitude of input strength I_0 for different values of κ using (4.42) and (4.43). Other parameters are $\kappa = 0.05$, $\alpha = 500$, $\beta = 0.01$, and $p = 6$. (Right) Double bump profile when $\kappa = 0.05$ and $I_0 = 0.4$.*

for the sign of perturbations at the bump boundaries, we obtain the following pseudolinear system characterizing the evolution of perturbations of the double bump solution:

$$\begin{aligned}\frac{\partial\psi_L(\theta,t)}{\partial t} &= -\psi_L(\theta,t) + \Phi_{Ll}(\theta,t) + \Phi_{Rc}(\theta,t) + \gamma_D w_l(\theta-\theta_1)\psi_L(\theta_1,t)G_{L,1}(t)\\ &\quad + \gamma_D w_l(\theta-\theta_2)\psi_L(\theta_2,t)G_{L,2}(t) + \gamma_D w_c(\theta+\theta_1)\psi_R(-\theta_1,t)G_{R,1}(t)\\ &\quad + \gamma_D w_c(\theta+\theta_2)\psi_R(-\theta_2,t)G_{R,2}(t), \qquad (4.44)\\ \frac{\partial\psi_R(\theta,t)}{\partial t} &= -\psi_R(\theta,t) + \Phi_{Rl}(\theta,t) + \Phi_{Lc}(\theta,t) + \gamma_D w_l(\theta+\theta_1)\psi_R(-\theta_1,t)G_{R,1}(t)\\ &\quad + \gamma_D w_l(\theta+\theta_2)\psi_R(-\theta_2,t)G_{R,2}(t) + \gamma_D w_c(\theta-\theta_1)\psi_1(\theta_1,t)G_{L,1}(t)\\ &\quad + \gamma_D w_c(\theta-\theta_2)\psi_L(\theta_2,t)G_{L,2}(t) \qquad (4.45)\end{aligned}$$

and

$$\begin{aligned}\frac{\partial\Phi_{Lm}(\theta,t)}{\partial t} &= -(\alpha^{-1}+\beta)\Phi_{Lm}(\theta,t)\\ &\quad - \beta(\gamma_D w_m(\theta-\theta_1)\psi_L(\theta_1,t)G_{L,1}(t)\Theta(\psi_L(\theta_1,t))\\ &\quad + \gamma_D w_m(\theta-\theta_2)\psi_L(\theta_2,t)G_{L,2}(t)\Theta(\psi_L(\theta_2,t))), \qquad (4.46)\\ \frac{\partial\Phi_{Rm}(\theta,t)}{\partial t} &= -(\alpha^{-1}+\beta)\Phi_{Rm}(\theta,t)\\ &\quad - \beta(\gamma_D w_m(\theta+\theta_1)\psi_R(-\theta_1,t)G_{R,1}(t)\Theta(\psi_R(-\theta_1,t))\\ &\quad + \gamma_D w_m(\theta+\theta_2)\psi_R(-\theta_2,t)G_{R,2}(t)\Theta(\psi_R(-\theta_2,t))), \qquad (4.47)\end{aligned}$$

where $G_{L,j}(t) = G(\psi_L(\theta_j,t)), G_{R,j}(t) = G(\psi_R(-\theta_j,t))$, and

$$\begin{aligned}(\gamma_D)^{-1} &= |U_L'(\theta_k)|\\ &= \frac{1}{1+\alpha\beta}\left|w_l(\theta_k-\theta_1) - w_l(\theta_k-\theta_2) + w_c(\theta_k+\theta_2) - w_c(\theta_k+\theta_1) + I_L'(\theta_k)\right|\\ &= |U_R'(-\theta_k)| \qquad (4.48)\\ &= \frac{1}{1+\alpha\beta}\left|w_l(\theta_k-\theta_2) - w_l(\theta_k-\theta_1) + w_c(\theta_k+\theta_1) - w_c(\theta_k+\theta_2) + I_R'(-\theta_k)\right|\end{aligned}$$

for $k = 1, 2$.

Equations (4.44)–(4.47) imply that the local stability of the stationary bump solution depends upon the spectral properties of a pseudolinear operator. As in section 4.2, we assume that (4.44)–(4.47) have separable solutions of the form $(\psi_L, \psi_R, \Phi_{1l}, \Phi_{2l}, \Phi_{Lc}, \Phi_{Rc})(\theta, t) = e^{\lambda t}(\psi_L, \psi_R, \Phi_{Ll}, \Phi_{Rl}, \Phi_{Lc}, \Phi_{Rc})(\theta)$, where λ is real. Under this assumption, the step functions Θ, G are time-independent so that $e^{\lambda t}$ cancels everywhere. Further simplification can be achieved by assuming that $\lambda \neq -(\alpha^{-1} + \beta)$ so that we can eliminate the auxiliary fields $\Phi_{Ll}, \Phi_{Rl}, \Phi_{Lc}, \Phi_{Rc}$. The resulting eigenvalue problem can be analyzed along similar lines to single bumps. That is, one particular class of solutions consists of functions $\psi_L(\theta)$ and $\psi_R(\theta)$ that vanish on the bump boundaries so that $\psi_L(\theta_1) = \psi_L(\theta_2) = \psi_R(-\theta_2) = \psi_R(-\theta_1) = 0$ and $\lambda = -1$. This determines the essential spectrum. The discrete spectrum is then found by setting $\theta = \pm\theta_1, \pm\theta_2$, which yields a four-dimensional matrix equation for the quantities $\psi_L(\theta_j), \psi_R(-\theta_j)$, $j = 1, 2$. Specifying the sign of these quantities thus yields sixteen classes of perturbation corresponding to all of the possible combinations of the perturbations for each individual bump: expansion, contraction, left-shift, and right-shift. However, there are only in fact seven qualitatively different cases due to symmetry considerations. We summarize these in Figure 14: (i) expand and contract (rivalry); (ii) same-shift; (iii) different-shift; (iv) expand-both; (v) contract-both; (vi) expand and shift; (vii) contract and shift. It is straightforward to numerically compute the eigenvalues associated with each perturbation after assigning the values for G and Θ due to the signs of each of the four points $\psi_L(\theta_1)$, $\psi_L(\theta_2)$, $\psi_R(-\theta_1)$, and $\psi_R(-\theta_2)$. We shall briefly summarize our findings for the eigenvalues associated with each perturbation followed by some specific examples.

(i) Expand and contract (rivalry), e.g., $\psi_L(\theta_{1,2}) > 0$ and $\psi_R(-\theta_{1,2}) < 0$. In the study of binocular rivalry, we are most interested in this perturbation, which expands one bump and contracts the other. For sufficiently small inputs I_0, we find that the double bump is unstable with respect to this class of perturbation as $\beta \to 0$. There are then three possibilities which we have found numerically: it destabilizes to the WTA solution (single bump), which occurs for weak synaptic depression; it destabilizes to damped oscillations which eventually return to the double bump solution; or it destabilizes to an indefinite rivalrous state of persistent oscillations, which occurs for sufficiently strong depression. Finally, if the input strength I_0 is large enough, we find that this is sufficient to stabilize the double bump solution with respect to rivalrous perturbations, as expected. When the double bump is linearly stable to rivalrous perturbations, there can coexist a state where the system persistently oscillates between either population possessing superthreshold activity. However, the initial conditions of the system must be sufficiently far away from the double bump solution.

(ii) Same-shift, e.g., $\psi_L(\theta_1) < 0, \psi_L(\theta_2) > 0$, $\psi_R(-\theta_2) < 0, \psi_R(-\theta_1) > 0$. We find that eigenvalues associated with this perturbation are always negative for sufficiently strong cross-inhibition ($w_0^c < 0$). However, as the amplitudes of the parameters w_0^c and w_2^c are reduced, it is possible to destabilize the double bump solution with respect to this perturbation, which numerically results in traveling pulse-like solutions in both hypercolumns that eventually settle back into the double bump solution.

(iii) Different-shift, e.g., $\psi_L(\theta_1) < 0, \psi_L(\theta_2) > 0$, $\psi_R(-\theta_2) > 0, \psi_R(-\theta_1) < 0$. We find that eigenvalues associated with this perturbation are always negative for sufficiently strong cross-inhibition ($w_0^c < 0$). However, as with case (ii), when the amplitude of the parameters w_0^c

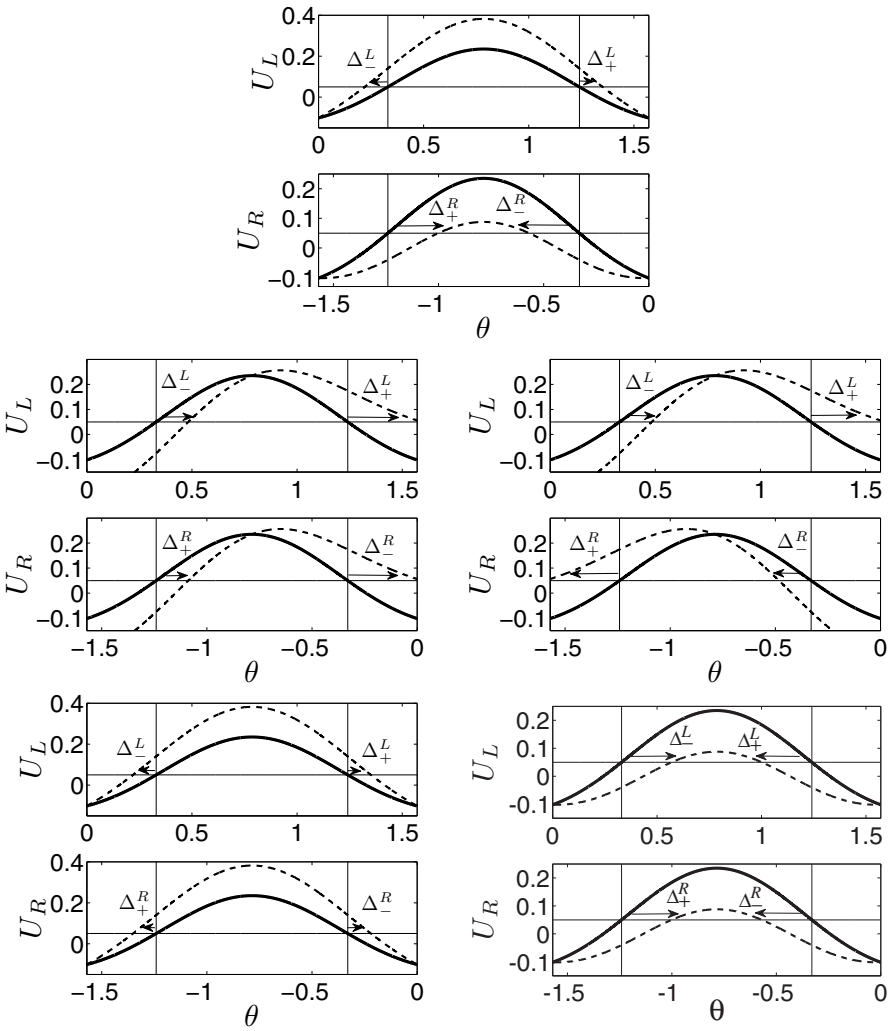

Figure 14. *Illustration of different types of perturbation of a stationary double-bump solution. (Top) expand and contract; (middle, left) right-shift both; (middle, right) left-shift and right-shift; (bottom, left) expand both; (bottom, right) contract both.*

and w_2^c is reduced, it is possible to destabilize the double bump solution, resulting in traveling pulse-like solutions in both hypercolumns that eventually settle back into the double bump solution.

(iv) Expand-both, e.g., $\psi_L(\theta_1) > 0, \psi_L(\theta_2) > 0$, $\psi_R(-\theta_2) > 0, \psi_R(-\theta_1) > 0$. Similar to cases (ii) and (iii), we find that this perturbation is stabilized by strong cross-inhibition but can lead to instability when w_0^c and w_2^c are sufficiently small in amplitude. However, due to periodicity, the spread of activity eventually settles back into the double bump solution.

(v) Contract-both, e.g., $\psi_L(\theta_1) < 0, \psi_L(\theta_2) < 0$, $\psi_R(-\theta_2) < 0, \psi_R(-\theta_1) < 0$. Due to the underlying symmetry of the system, we can in fact compute the eigenvalue associated with this perturbation explicitly. Noting the sign restrictions and the fact that we must have

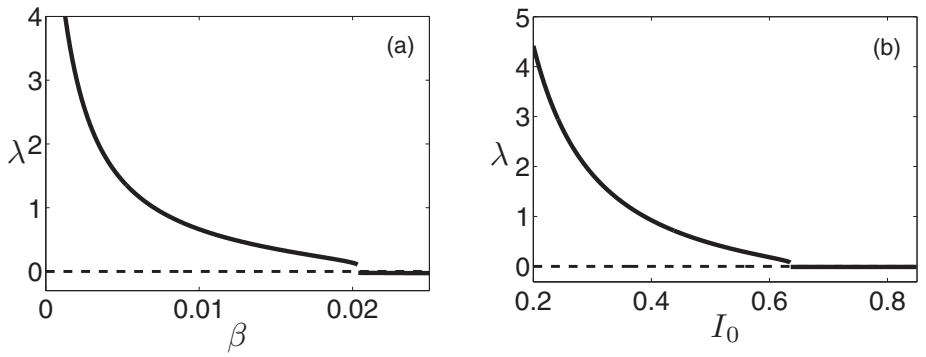

Figure 15. *Eigenvalues associated with expand and contract (rivalrous) perturbations of double bump (case* (i)*).* (a) *Maximal nonzero eigenvalue plotted as a function of* β *for fixed* $I_0 = 0.45$. (b) *Maximal nonzero real eigenvalues plotted as a function of* I_0 *for* $\beta = 0.01$. *Other parameters are* $\kappa = 0.05$, $w_0^l = 0$, $w_2^l = 0.4$, $w_0^c = -1$, $w_2^c = 0.5$, *and* $\alpha = 500$.

$\psi_L(\theta_1) = \psi_L(\theta_2) = \psi_R(-\theta_2) = \psi_R(-\theta_1) < 0$, we have

$$\lambda = -1 + \frac{\gamma_D}{1+\alpha\beta}(w_l(0) + w_l^- + w_c(2\theta_1) + w_c^+), \tag{4.49}$$

which we find to always be negative as long as $w_0^c \leq 0$. Thus, the bump will always be stable with respect to contractions. In fact, this seems to be what allows the system to settle back into the double bump solution after a long excursion due to a destabilizing perturbation, since there are flows that treat the double bump as an attractor.

(vi) Expand and shift, e.g., $\psi_L(\theta_1) > 0, \psi_L(\theta_2) > 0$, $\psi_R(-\theta_2) < 0, \psi_R(-\theta_1) > 0$. We find no eigensolutions of this form for any parameters.

(vii) Contract and shift, e.g., $\psi_L(\theta_1) < 0, \psi_L(\theta_2) < 0$, $\psi_R(-\theta_2) < 0, \psi_R(-\theta_1) > 0$. We find no eigensolutions of this form for any parameters.

We illustrate the stability analysis of the stationary double bump solution by plotting eigenvalues calculated for each perturbation to bumps in a network with the harmonic weight function (2.4). Specifically, we plot the eigenvalues for each perturbation for a stimulus driven double bump that is unstable to rivalrous perturbations as $\beta \to 0$. In Figure 15, we plot the maximal nonzero real eigenvalue for rivalrous perturbations as a function of β and I_0. For fixed I_0, as β increases from zero the positive real eigenvalue decreases as a function of β. For sufficiently large β, this positive eigenvalue vanishes, and the double bump solution is predicted to be stable to rivalrous perturbations. For fixed β, double bumps are unstable to rivalrous perturbations for sufficiently weak inputs but stabilize beyond a critical value of I_0. In Figure 16, we plot the maximal eigenvalues of all other perturbations to the bump, showing they are negative for a wide range of input strengths I_0 and depression strengths β. They are all quite insensitive to variations in these parameters.

5. Numerical simulations.

We now study the full system (2.1) using a numerical approximation scheme. To evolve the system in time, we use a fourth order Runge–Kutta method with 1000–2000 spatial grid points and a time step of $dt = 0.01$. The integral terms in (2.1a) and (2.1b) are approximated using Simpson's rule. We systematically checked whether taking

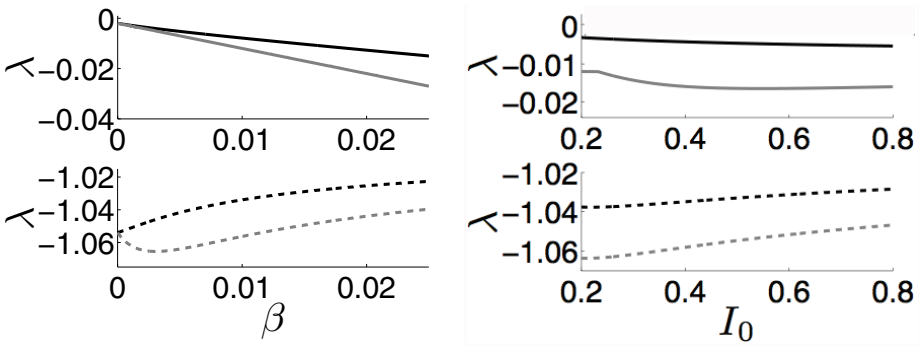

Figure 16. *Eigenvalues associated with other perturbations of double bump (cases* (ii)–(v)*). (Left) Maximal real eigenvalues of the expand-both (solid black), contract-both (dashed black), same-shift (solid grey), and different-shift (dashed grey) perturbations plotted as a function of* β *for fixed* $I_0 = 0.45$*. (Right) Maximal real eigenvalues of each perturbation plotted as a function of* I_0 *for* $\beta = 0.01$*. Other parameters are* $\kappa = 0.05$*,* $w_0^l = 0$*,* $w_2^l = 0.4$*,* $w_0^c = -1$*,* $w_2^c = 0.5$*, and* $\alpha = 500$*.*

finer grids changed stability results, and it does not. Such checks are essential to studying the stability of bumps, as grids that are too coarse can drastically alter stability results [27].

In much of parameter space, we find that our existence and stability analysis characterizes very well the type of solutions that the system (2.1) will relax to over long times as well as the nature of various local instabilities. Thus, if we take as an initial condition a stationary bump solution that is stable with respect to perturbations associated with real eigenvalues and then vary a bifurcation parameter such as β or I_0, we find that the dominant instability, as predicted by our piecewise smooth analysis, corresponds well with the numerical solution seen initially to evolve away from the stationary solution. However, one interesting feature we find in numerical simulations of the network is that solutions that destabilize initially can eventually return to a stationary solution. This is due to two features of the underlying system and associated stationary solution. First, the bump is stable with respect to certain perturbations in our piecewise linear stability analysis. Therefore, even though the solution may move away from a stationary bump when one perturbation is applied, it may follow a trajectory in phase space which is eventually close to the stationary bump solution again. This phenomenon is aided by the second effect, which is that the variables $q_j(\theta, t)$ as defined by (2.1c) reduce their value at a location quite quickly when the superthreshold activity of $u_j(\theta, t)$ sweeps over that location in the network. Thus, $q_j(\theta, t)$ will be lower than the value prescribed by the stationary solutions on the regions immediately exterior to the original bump location following the bump. This effect will last for long periods of time since α is large. Therefore, in some situations there will not be enough resources in the regions about the bump's original location to reignite the instability once the activity profile returns to the general proximity of the bump. We shall witness this phenomenon in both single and double bump instabilities.

For our first numerical example, we take the initial condition to be a single bump solution specified by (4.8) which is predicted to be unstable to shift perturbations. After a brief period,

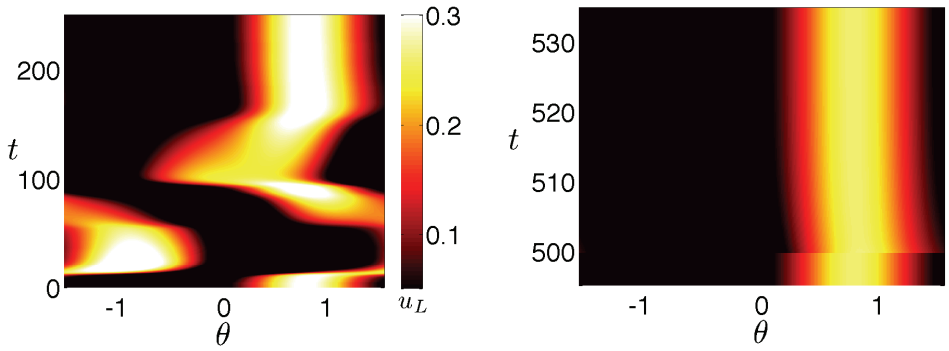

Figure 17. *Numerical simulation of a single bump destabilized by a rightward shift perturbation. (Left) Simulation in the network (2.1) with a Heaviside firing rate function (2.3). Plot of $u_L(\theta,t)$ for an initial condition taken to be a stationary bump specified by (4.8). Solution is perturbed at $t=5$ by a rightward shift $\psi_L^{shift}(\theta,t)$ such that $\chi(t)=0.02$ for $t\in[5,5.1)$ and zero otherwise. Activity initially propagates rightward and then leftward until settling back into the single bump profile. (Right) Simulation in the network (2.1) with a smooth sigmoidal firing rate function (2.2) with gain $\eta=20$. System is allowed to evolve for 500 time units from the single bump solution of the nearby system with a Heaviside function (2.3) until it settles into its own single bump solution. The system is then perturbed at $t=500$ by a rightward shift $\psi_L^{shift}(\theta,t)$ such that $\chi(t)=0.02$ for $t\in[500,500.1)$ and zero otherwise. Activity relaxes back to the single bump solution immediately. Other parameters are $\kappa=0.05$, $w_0^l=0$, $w_2^l=0.4$, $w_0^c=-1$, $w_2^c=0.5$, $\alpha=500$, $\beta=0.01$, $I_0=0.24$. Each t time unit corresponds to $10ms$.*

we perturb the system by adding a rightward shift perturbation of $u_L(\theta,t)$ defined as

$$\psi_L^{shift}(\theta,t)=\chi(t)(w_l(\theta-\theta_2)-w_l(\theta-\theta_1)), \tag{5.1}$$

where $\chi(t)$ is a time-dependent function determining when and for how long the perturbation is applied. As shown in Figure 17(left), the resulting dynamics initially evolve to a propagating solution similar to a traveling pulse. However, due to the input and periodic boundaries of the system, the profile does not evolve to a translationally invariant traveling pulse as in our previous studies of a network with synaptic depression [36, 12]. In fact, the activity then changes its direction of propagation. Following its excursion, the activity profile eventually settles back into the stationary single bump solution. As mentioned earlier, the trajectory of the variable $u_L(\theta,t)$ is such that it relaxes back to the bump solution through a stable flow. Since the piecewise-smooth boundary of the variables $q_j(\theta,t)$ has been disrupted by nonlinear effects of the evolving solution, the bump will be an attracting state for virtually all reasonable flows over a long time. It appears the single bump is a marginally stable steady state in the infinite dimensional system (2.1). Thus, even though the bump is unstable to shift perturbations, it always restabilizes in the long time limit. It is then reasonable to ask whether such trajectories found in system (2.1) with a Heaviside firing rate function (2.3) are nongeneric or if it is possible to find similar behavior in the system with a smooth sigmoid firing rate function (2.2). When simulating the nearby system with a sigmoid with high gain, we find similar dynamics. Once the system settles into a single bump solution, small perturbations lead to similar excursions followed by a return to the original steady state. We found, however, that there is a critical size of perturbation that leads to such

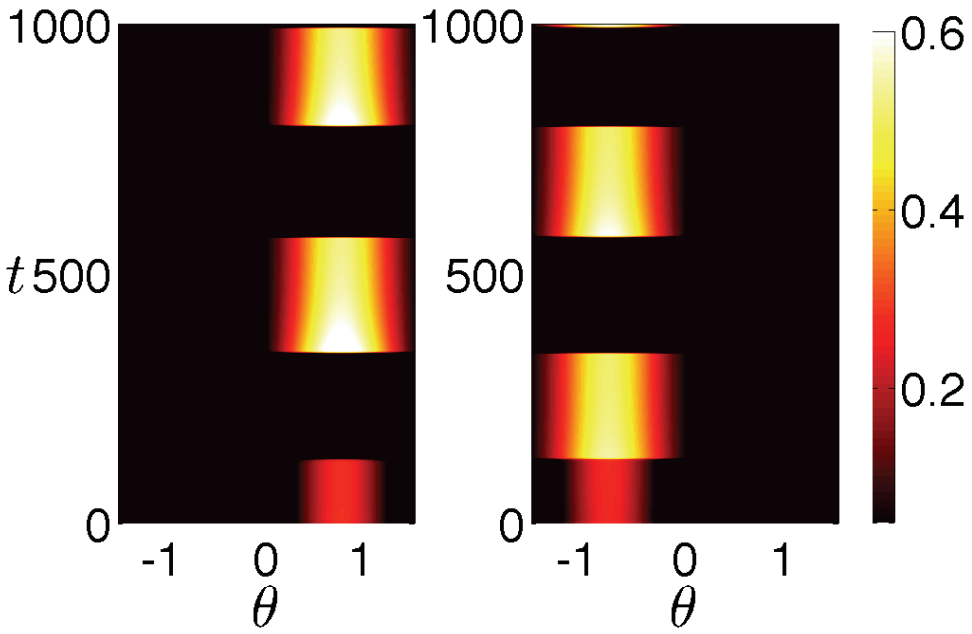

Figure 18. *Numerical simulation of a double bump destabilized by a rivalrous perturbation. Plot of* $u_L(\theta,t)$ *(left) and* $u_R(\theta,t)$ *(right) for an initial condition taken to be a double bump specified by* (4.40) *and* (4.41)*. Solution is perturbed at* $t = 5$ *by a rivalry shift* $\psi_L^{riv}(\theta,t)$ *and* $\psi_R^{riv}(\theta,t)$*, respectively, such that* $\chi(t) = 0.02$ *for* $t \in [5, 5.1)$ *and zero otherwise. Activity settles into a slow oscillation where dominance switches between either population roughly every two seconds. Parameters are* $\kappa = 0.05$*,* $w_0^l = 0$*,* $w_2^l = 0.4$*,* $w_0^c = -1$*,* $w_2^c = 0.5$*,* $\alpha = 500$*,* $\beta = 0.01$*, and* $I_0 = 0.45$*. Each* t *time unit corresponds to* $10ms$*.*

an excursion. Smaller perturbations lead to the solutions immediately relaxing back to a single bump. We found this was not a grid size effect, as reducing the grid size did not alter the size of perturbation necessary to destabilize the bump. Therefore, as we have found in previous work for networks with smooth sigmoids with large gain, bumps may be stable to extremely small perturbations, but not necessarily stable for slightly larger perturbations that are still relatively small [37]. However, we did find that this effect eventually vanishes when the smooth sigmoid has moderate gain. When we simulate the nearby system with a sigmoid with gain $\eta = 20$, we find that the bump simply behaves as a stable structure, so that even large perturbations decay. This is shown in Figure 17(right), where a shifted bump relaxes back to the original stable structure.

For our next numerical example, we take the initial condition to be a double bump solution specified by (4.40) and (4.41), which is predicted to be unstable to rivalrous perturbations. After a brief period, we perturb the system by adding a rivalrous perturbation of $u_L(\theta,t)$ and $u_R(\theta,t)$ defined as

$$\psi_L^{riv}(\theta,t) = \chi(t)(w_l(\theta-\theta_2) + w_l(\theta-\theta_1)), \tag{5.2}$$

$$\psi_R^{riv}(\theta,t) = -\chi(t)(w_l(\theta+\theta_2) + w_l(\theta+\theta_1)). \tag{5.3}$$

As shown in Figure 18, the resulting dynamics can evolve to a slow oscillation in the activ-

ity of both populations for sufficiently weak inputs I_0. First the right population's activity $u_R(\theta,t)$ exhibits a relatively invariant bump of activity until synaptic depression exhausts the inhibitory synapses and the left population's activity $u_L(\theta,t)$ is released from suppression. Then the left population's activity dominates for a period until the right population is released. This cycle continues indefinitely. Thus, even though the linear stability analysis predicts the rivalrous perturbation having an associated positive real eigenvalue (see Figure 15), nonlinear effects of the system take over and the system oscillates. As we alluded to in section 4.4, the spatially extended system supports a fusion/rivalry bistable state, just as the space-clamped system of section 3 does. Thus, even in cases where the double bump solution is linearly stable, some initial conditions evolve to a rivalry solution similar to that plotted in Figure 18. Interestingly, Buckthought, Kim, and Wilson have recently provided psychophysical evidence for such a form of bistability [14]. By showing subjects' binocular stimuli with increasingly dissimilar orientations, they found a region of hysteresis, wherein the subject perceived either rivalry or fusion, depending on their initial perception. Admittedly, the stimuli used to induce the effect never differed more than 30 degrees, whereas ours differ by 90 degrees, but they observed such bistability nonetheless. To study the effect that the gain of the firing rate function has upon such rivalry solutions, we study rivalrous oscillations in system (2.1) with the smooth sigmoid firing rate function (2.2) with gain $\eta = 30$. By allowing the system to evolve from the double bump solution of the nearby Heaviside system, we find that it eventually settles into rivalrous oscillations. This is illustrated in Figure 19, which shows rivalrous oscillations that switch between population dominance roughly every 2 seconds (200 time units). Thus, the dynamics we find in system (2.1) with a Heaviside firing rate function (2.3) persist in the case of a sigmoid firing rate function with large but finite gain.

In Figure 20, we show an example of a perturbation evolving to a damped oscillation. Even though our stability analysis predicts that the double bump is unstable with respect to rivalrous perturbations, the solution eventually returns to the stationary double bump. As we have mentioned, double bumps can be stable to all other perturbations aside from the rivalrous perturbation. Therefore, nonlinear effects can dominate the system in the long time limit and the solution may flow along a trajectory which has the double bump as an attractor. As mentioned previously, resources as defined by $q_j(\theta,t)$ in the periphery of the original bump locations are exhausted so that there is not sufficient excitation to continue the oscillation. In addition, we cannot trust the stability analysis we have carried out beyond the point that the original threshold conditions are violated. To our knowledge, no studies have addressed these types of nonlinear effects at work in restabilizing bumps in spatially extended systems. How best to characterize the onset of such an oscillation remains an open problem.

Finally, in Figure 21, we show an example of a coupled hypercolumn network driven by stimuli of two different strengths so that $I_L \neq I_R$. We take our initial condition to be the quiescent state $u_L(\theta,0) = u_R(\theta,0) = 0$ and $q_L(\theta,t) = q_R(\theta,0) = 1$. In this case, we see that the dominance times are different for the left and right populations, just as we found in the space-clamped system (see Figure 3). Since the right population receives a stronger input ($I_R = 0.45$) than the left population ($I_L = 0.4$), superthreshold bump-like activity exists in the right population for a longer period than the left. Also, note that the transient bump in the right population is wider than that in the left.

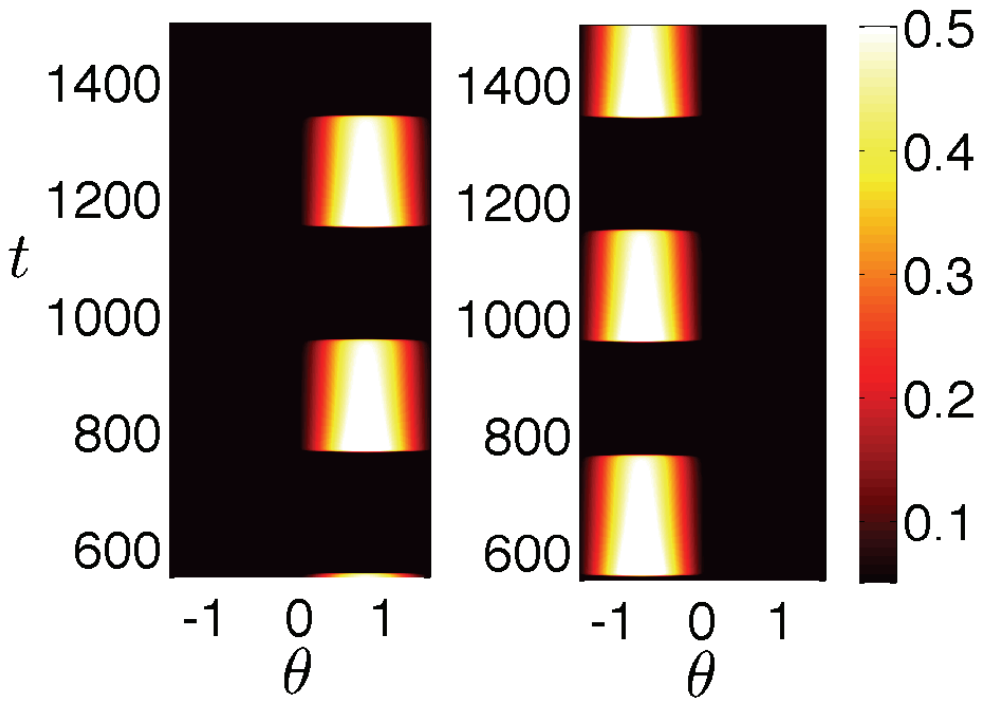

Figure 19. *Numerical simulation of a double bump destabilized by a rivalrous perturbation in system (2.1) with a sigmoid firing rate (2.2) with gain $\eta = 30$. Plot of $u_L(\theta,t)$ (left) and $u_R(\theta,t)$ (right) for an initial condition taken to be a double bump specified by (4.40) and (4.41) for the nearby system with a Heaviside firing rate (2.3). Activity evolves eventually into a slow oscillation where dominance switches between either population roughly every two seconds. Other parameters are $\kappa = 0.05$, $w_0^l = 0$, $w_2^l = 0.4$, $w_0^c = -1$, $w_2^c = 0.5$, $\alpha = 500$, $\beta = 0.01$, and $I_0 = 0.45$. Each t time unit corresponds to $10ms$.*

6. Discussion. In this paper, we analyzed the onset of binocular rivalrous oscillations in a coupled hypercolumn model with synaptic depression. In order to facilitate our analysis we took the firing rate function to be a Heaviside (2.3). However, it was then necessary to take the piecewise nature of the system into account when analyzing the stability of stationary solutions. We first calculated the period of rivalrous oscillations arising in the space-clamped version of our model. When the input to the left and right eye populations was varied, we found that the corresponding changes in dominance times matched very well with some of the observations of binocular rivalry made by Levelt [45]. Then, by studying the effects of additive noise in the model, we found realistic statistics for dominance duration distributions when noise is included in the equations for the depression variables. In the spatially extended version of our model, we analyzed the onset of oscillations in neural activity due to orientation biased stimuli using local stability determined by the spectrum of a pseudolinear operator. For WTA or single bump solutions, we found that the dominant instability was usually a shifting of the bump boundary, which in numerical simulations led to traveling pulse-type solutions. For fusion or double bump solutions, we found that the dominant instability was an expansion of one bump and a contraction of the other, which in simulations often led

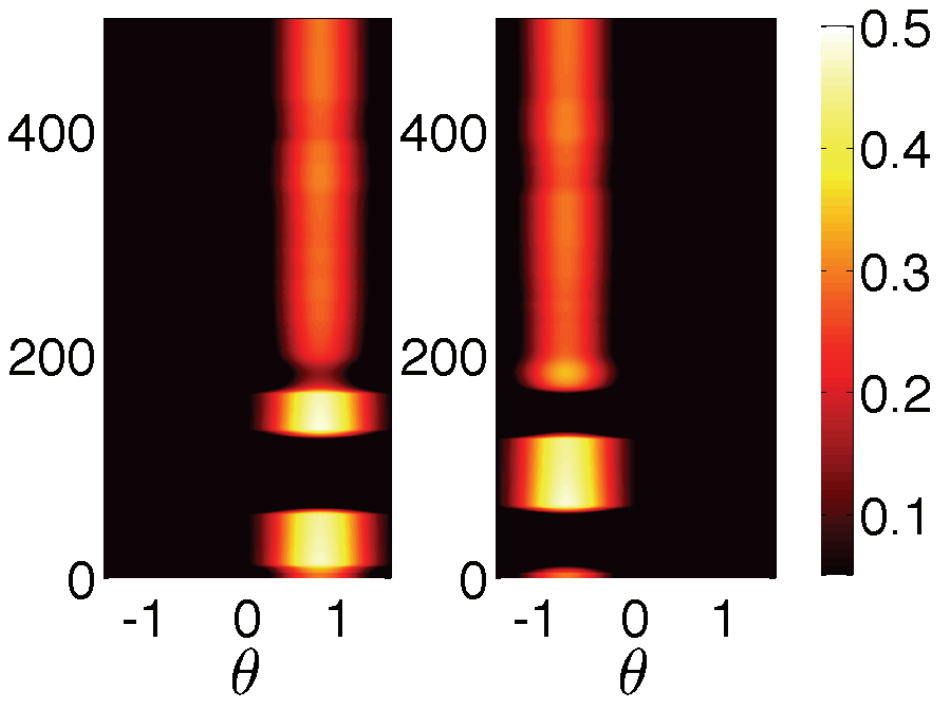

Figure 20. *Numerical simulation of a double bump destabilized by a rivalrous perturbation in system (2.1) with a Heaviside firing rate (2.3). Plot of $u_L(\theta,t)$ (left) and $u_R(\theta,t)$ (right) for an initial condition taken to be a double bump specified by (4.40) and (4.41). Solution is perturbed at $t=5$ by a rivalry shift $\psi_L^{riv}(\theta,t)$ and $\psi_R^{riv}(\theta,t)$, respectively, such that $\chi(t)=0.02$ for $t\in[5,5.1)$ and zero otherwise. Activity evolves to a damped oscillation temporarily and then settles back into the stationary double bump. Parameters are $\kappa=0.05$, $w_0^l=0$, $w_2^l=0.4$, $w_0^c=-1$, $w_2^c=0.5$, $\alpha=500$, $\beta=0.02$, and $I_0=0.4$. Each t time unit corresponds to $10ms$.*

to rivalrous oscillations. In numerical simulations, we found that the local stability analysis predicted the point at which bump solutions destabilized, but the long time behavior of the simulation is beyond the scope of our analysis.

In future work, it would be interesting to develop tools to analyze the long time behavior of oscillations in the spatially extended system so we could compute the dominance times of each population. In addition, the fact that piecewise-smooth analysis predicts that a bump can be stable to one sign of perturbation and unstable to another sign of perturbation was borne out in the results of our numerical simulations. It appears this behavior allows the bump to be a starting and stopping point for homoclinic trajectories in the infinite dimensional system (2.1). In a sense, the bump is marginally stable. This was not an issue when we studied instabilities of bumps in a network with synaptic depression without periodic boundaries [12]. We would like to explore this notion more exactly using tools developed for the study of piecewise-smooth dynamical systems [21].

Appendix. To calculate the stability of the double bump and derive the set of equations (4.44)–(4.47), we begin by letting $u_j(\theta,t)=U_j(\theta)+\varepsilon\psi_j(\theta,t)$ and $q_j(\theta,t)=Q_j(\theta)+\varepsilon\varphi_j(\theta,t)$ for $j=L,R$, where ψ_j and φ_j denote smooth perturbations and $\varepsilon\ll 1$. Substituting into the

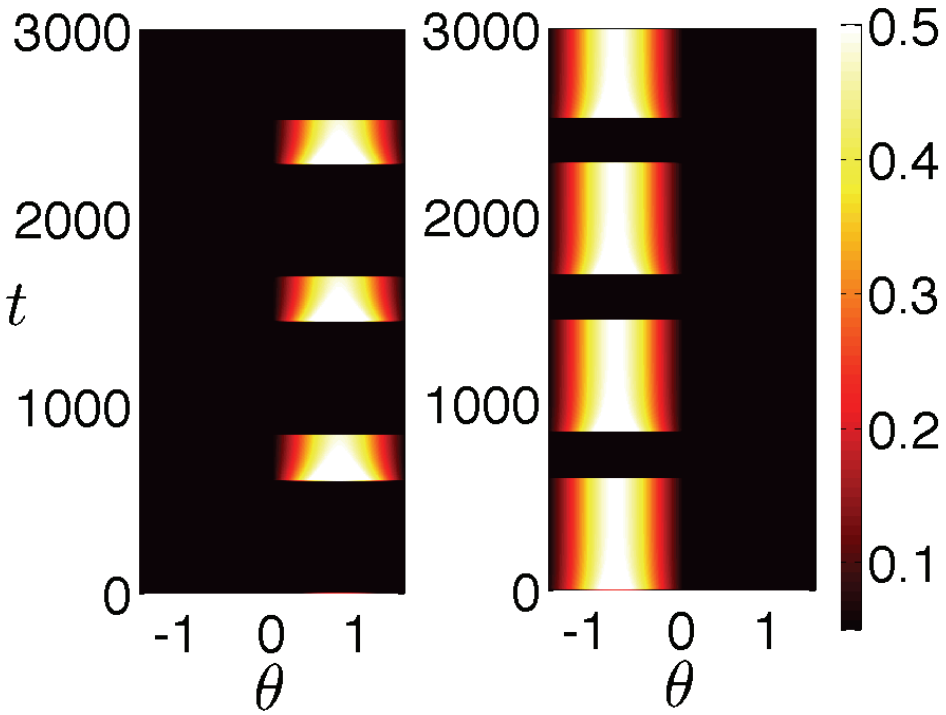

Figure 21. *Numerical simulation of an asymmetric rivalrous solution. Plot of $u_L(\theta,t)$ (left) and $u_R(\theta,t)$ (right) for an initial condition taken to be the quiescent state $u_L(\theta,0)=u_R(\theta,0)=0$ and $q_L(\theta,t)=q_R(\theta,0)=1$. Activity evolves to a damped oscillation temporarily and then settles back into the stationary double bump. Parameters are $\kappa=0.05$, $w_0^l=0$, $w_2^l=0.4$, $w_0^c=-1$, $w_2^c=0.5$, $\alpha=500$, $\beta=0.01$, $I_L^0=0.4$, and $I_R^0=0.45$. Each t time unit corresponds to $10ms$.*

full system (2.1), imposing the stationary solutions (4.35), (4.36), and (4.37), and dividing through by ε then gives

$$\begin{aligned}\frac{\partial\psi_L(\theta,t)}{\partial t} &= -\psi_L(\theta,t)+\frac{1}{\varepsilon}w_l*(Q_L[\Theta(U_L+\varepsilon\psi_L-\kappa)-\Theta(U_L-\kappa)])\\ &\quad + w_l*(\varphi_L\Theta(U_L+\varepsilon\psi_L-\kappa))+w_c*(\varphi_R\Theta(U_R+\varepsilon\psi_R-\kappa))\\ &\quad +\frac{1}{\varepsilon}w_c*(Q_R[\Theta(U_R+\varepsilon\psi_R-\kappa)-\Theta(U_R-\kappa)]),\end{aligned}\tag{A.1}$$

$$\begin{aligned}\frac{\partial\psi_R(\theta,t)}{\partial t} &= -\psi_R(\theta,t)+\frac{1}{\varepsilon}w_l*(Q_R[\Theta(U_R+\varepsilon\psi_R-\kappa)-\Theta(U_R-\kappa)])\\ &\quad + w_l*(\varphi_R\Theta(U_R+\varepsilon\psi_R-\kappa))+w_c*(\varphi_L\Theta(U_L+\varepsilon\psi_L-\kappa))\\ &\quad +\frac{1}{\varepsilon}w_c*(Q_L[\Theta(U_L+\varepsilon\psi_L-\kappa)-\Theta(U_L-\kappa)]),\end{aligned}\tag{A.2}$$

$$\frac{\partial\varphi_j(\theta,t)}{\partial t} = -\frac{\varphi_j(\theta,t)}{\alpha}-\frac{\beta}{\varepsilon}Q_j[\Theta(U_j+\varepsilon\psi_j-\kappa)-\Theta(U_j-\kappa)]-\beta\varphi_j\Theta(U_j+\varepsilon\psi_j-\kappa)\tag{A.3}$$

for $j = L, R$. Denote the perturbations of the bump boundaries by $\varepsilon\Delta_{\pm}^{L}(t)$ and $\varepsilon\Delta_{\pm}^{R}$ such that

$$u_L(\theta_1 + \varepsilon\Delta_-^L(t), t) = u_L(\theta_2 + \varepsilon\Delta_+^L(t), t) = \kappa, \tag{A.4}$$

$$u_R(-\theta_1 + \varepsilon\Delta_-^R(t), t) = u_R(-\theta_2 + \varepsilon\Delta_+^R(t), t) = \kappa \tag{A.5}$$

for an initial time interval $t \in [0, T)$. We are especially interested in perturbations that violate these threshold conditions eventually (after time T), since this is precisely what occurs in the case of rivalrous oscillations. Taylor expanding these threshold conditions to first order in perturbations, we find that

$$\begin{aligned} \Delta_-^L(t) &\approx -\frac{\psi_L(\theta_1, t)}{|U_L'(\theta_1)|}, \quad \Delta_+^L(t) \approx \frac{\psi_L(\theta_2, t)}{|U_L'(\theta_2)|}, \\ \Delta_-^R(t) &\approx \frac{\psi_R(-\theta_1, t)}{|U_R'(-\theta_1)|}, \quad \Delta_+^R(t) \approx -\frac{\psi_R(-\theta_2, t)}{|U_R'(-\theta_2)|}. \end{aligned} \tag{A.6}$$

As in the single bump case, we can smooth out discontinuities in (A.3) by introducing the fields

$$\Phi_{Lm}(\theta, t) = \int_{\theta_1 + \varepsilon\Delta_-^L}^{\theta_2 + \varepsilon\Delta_+^L} w_m(\theta - \theta')\varphi_L(\theta', t)\mathrm{d}\theta', \tag{A.7}$$

$$\Phi_{Rm}(\theta, t) = \int_{-\theta_2 + \varepsilon\Delta_+^R}^{-\theta_1 + \varepsilon\Delta_-^R} w_m(\theta - \theta')\varphi_R(\theta', t)\mathrm{d}\theta' \tag{A.8}$$

for $m = l, c$. Thus, as in the single bump case, even though $\mathcal{O}(1/\varepsilon)$ pointwise changes in $\varphi_L(\theta, t)$ and $\varphi_R(\theta, t)$ may occur, the bump solution may still be stable, since the region over which $\mathcal{O}(1/\varepsilon)$ changes occur may shrink to zero. We account for this possibility, since the dynamics of the fields $\Phi_{Lm}(\theta, t)$ and $\Phi_{Rm}(\theta, t)$ $(m = l, c)$ will remain $\mathcal{O}(1)$ when $\varphi_L(\theta, t)$ and $\varphi_R(\theta, t)$ are $\mathcal{O}(1/\varepsilon)$ over an infinitesimal interval.

If we now differentiate (A.7) and (A.8) with respect to time, we find

$$\begin{aligned} \frac{\partial\Phi_{Lm}(\theta, t)}{\partial t} &= \int_{\theta_1 + \varepsilon\Delta_-^L}^{\theta_2 + \varepsilon\Delta_+^L} w_m(\theta - \theta')\frac{\partial\varphi_L(\theta', t)}{\partial t}\mathrm{d}\theta' \\ &\quad + \varepsilon w_m(\theta - \theta_2 - \varepsilon\Delta_+^L(t))\varphi_L(\theta_2 + \varepsilon\Delta_+^L(t), t)\dot{\Delta}_+^L(t) \\ &\quad - \varepsilon w_m(\theta - \theta_1 - \varepsilon\Delta_-^L(t))\varphi_L(\theta_1 + \varepsilon\Delta_-^L(t), t)\dot{\Delta}_-^L(t), \qquad m = l, c, \end{aligned} \tag{A.9}$$

$$\begin{aligned} \frac{\partial\Phi_{Rm}(\theta, t)}{\partial t} &= \int_{-\theta_2 + \varepsilon\Delta_+^R}^{-\theta_1 + \varepsilon\Delta_-^R} w_m(\theta - \theta')\frac{\partial\varphi_R(\theta', t)}{\partial t}\mathrm{d}\theta' \\ &\quad + \varepsilon w_m(\theta + \theta_1 - \varepsilon\Delta_-^R(t))\varphi_R(-\theta_1 + \varepsilon\Delta_-^R(t), t)\dot{\Delta}_-^R(t) \\ &\quad - \varepsilon w_m(\theta + \theta_2 - \varepsilon\Delta_+^R(t))\varphi_R(-\theta_2 + \varepsilon\Delta_+^R(t), t)\dot{\Delta}_+^R(t), \qquad m = l, c, \end{aligned} \tag{A.10}$$

where $\dot{\Delta}_{\pm}^{j} = \mathrm{d}\Delta_{\pm}^{j}/\mathrm{d}t$ $(j = L, R)$. We can now substitute (A.3) for $\partial\varphi_j/\partial t$ $(j = L, R)$. Note that the final term in (A.3) for $j = L$ $(j = R)$ involves a Heaviside function which will be nonzero only when the stationary bumps U_L (U_R) plus the perturbation $\varepsilon\psi_L$ $(\varepsilon\psi_R)$ is greater

than the threshold κ. This region is precisely defined by the interval $(\theta_1+\varepsilon\Delta_-^L, \theta_2+\varepsilon\Delta_+^L)$ (interval $(-\theta_2+\varepsilon\Delta_+^R, -\theta_1+\varepsilon\Delta_-^R)$), over which the integral in (A.9) (equation (A.10)) is taken. This implies that

$$\int_{\theta_1+\varepsilon\Delta_-^L}^{\theta_2+\varepsilon\Delta_+^L} w_m(\theta-\theta')\varphi_L(\theta',t)\Theta(U_L(\theta',t)+\varepsilon\varphi_L(\theta',t)-\kappa)\mathrm{d}\theta' = \Phi_{Lm}(\theta,t),$$
$$\int_{-\theta_2+\varepsilon\Delta_+^R}^{-\theta_1+\varepsilon\Delta_-^R} w_m(\theta-\theta')\varphi_R(\theta',t)\Theta(U_L(\theta',t)+\varepsilon\varphi_R(\theta',t)-\kappa)\mathrm{d}\theta' = \Phi_{Rm}(\theta,t).$$

Thus, by modifying (A.1), (A.2), and (A.3) with the auxiliary variables given in (A.9) and (A.10), we have the alternative system of equations

$$\begin{aligned}(\text{A.11})\quad \frac{\partial\psi_L(\theta,t)}{\partial t} &= -\psi_L(\theta,t)+\Phi_{Ll}(\theta,t)+\Phi_{Rc}(\theta,t)\\ &\quad+\frac{1}{\varepsilon}\int_{\theta_1+\varepsilon\Delta_-^L(t)}^{\theta_2+\varepsilon\Delta_+^L(t)} w_l(\theta-\theta')Q_L(\theta')\mathrm{d}\theta'-\frac{1}{\varepsilon}\int_{\theta_1}^{\theta_2} w_l(\theta-\theta')Q_L(\theta')\mathrm{d}\theta'\\ &\quad+\frac{1}{\varepsilon}\int_{-\theta_2+\varepsilon\Delta_+^R(t)}^{-\theta_1+\varepsilon\Delta_-^R(t)} w_c(\theta-\theta')Q_R(\theta')\mathrm{d}\theta'-\frac{1}{\varepsilon}\int_{-\theta_2}^{-\theta_1} w_c(\theta-\theta')Q_R(\theta')\mathrm{d}\theta',\end{aligned}$$

$$\begin{aligned}(\text{A.12})\quad \frac{\partial\psi_L(\theta,t)}{\partial t} &= -\psi_R(\theta,t)+\Phi_{Rl}(\theta,t)+\Phi_{Lc}(\theta,t)\\ &\quad+\frac{1}{\varepsilon}\int_{-\theta_2+\varepsilon\Delta_+^R(t)}^{-\theta_1+\varepsilon\Delta_-^R(t)} w_l(\theta-\theta')Q_R(\theta')\mathrm{d}\theta'-\frac{1}{\varepsilon}\int_{-\theta_2}^{-\theta_1} w_l(\theta-\theta')Q_R(\theta')\mathrm{d}\theta'\\ &\quad+\frac{1}{\varepsilon}\int_{\theta_1+\varepsilon\Delta_-^L(t)}^{\theta_2+\varepsilon\Delta_+^L(t)} w_c(\theta-\theta')Q_L(\theta')\mathrm{d}\theta'-\frac{1}{\varepsilon}\int_{\theta_1}^{\theta_2} w_c(\theta-\theta')Q_L(\theta')\mathrm{d}\theta',\end{aligned}$$

$$\begin{aligned}(\text{A.13})\quad \frac{\partial\Phi_{Lm}(\theta,t)}{\partial t} &= -(\alpha^{-1}+\beta)\Phi_{Lm}(\theta,t)\\ &\quad-\frac{\beta}{\varepsilon}\int_{\theta_1+\varepsilon\Delta_-^L(t)}^{\theta_2+\varepsilon\Delta_+^L(t)} w_m(\theta-\theta')Q_L(\theta')[\Theta(U_L+\varepsilon\psi_L-\kappa)-\Theta(U_L-\kappa)]\mathrm{d}\theta\\ &\quad+\varepsilon w_m(\theta-\theta_2-\varepsilon\Delta_+^L(t))\varphi_L(\theta_2+\varepsilon\Delta_+^L(t),t)\dot{\Delta}_+^L(t)\\ &\quad-\varepsilon w_m(\theta-\theta_1-\varepsilon\Delta_-^L(t))\varphi_L(\theta_1+\varepsilon\Delta_-^L(t),t)\dot{\Delta}_-^L(t),\qquad m=l,c,\end{aligned}$$

$$\begin{aligned}(\text{A.14})\quad \frac{\partial\Phi_{Rm}(\theta,t)}{\partial t} &= -(\alpha^{-1}+\beta)\Phi_{Rm}(\theta,t)\\ &\quad-\frac{\beta}{\varepsilon}\int_{-\theta_2+\varepsilon\Delta_+^R(t)}^{-\theta_1+\varepsilon\Delta_-^R(t)} w_m(\theta-\theta')Q_R(\theta')[\Theta(U_R+\varepsilon\psi_R-\kappa)-\Theta(U_R-\kappa)]\mathrm{d}\theta\\ &\quad-\varepsilon w_m(\theta+\theta_2-\varepsilon\Delta_+^R(t))\varphi_R(-\theta_2+\varepsilon\Delta_+^R(t),t)\dot{\Delta}_+^R(t)\\ &\quad+\varepsilon w_m(\theta+\theta_1-\varepsilon\Delta_-^R(t))\varphi_R(-\theta_1+\varepsilon\Delta_-^R(t),t)\dot{\Delta}_-^R(t),\qquad m=l,c.\end{aligned}$$

We can now linearize the system of equations (A.11), (A.12), (A.13), and (A.14) by expanding in powers of ε and collecting all $\mathcal{O}(1)$ terms. Again it is important to keep track of the signs of $\Delta_{\pm}^{L}$ and $\Delta_{\pm}^{R}$ when approximating the various integrals due to the discontinuous nature of $Q_L(\theta)$ and $Q_R(\theta)$. We thus obtain the following pseudolinear system:

$$\begin{aligned}\frac{\partial \psi_L(\theta,t)}{\partial t} &= -\psi_L(\theta,t)+\Phi_{Ll}(\theta,t)+\Phi_{Rc}(\theta,t)+\gamma_D w_l(\theta-\theta_1)\psi_L(\theta_1,t)G_{L,1}(t)\\ &\quad+\gamma_D w_l(\theta-\theta_2)\psi_L(\theta_2,t)G_{L,2}(t)+\gamma_D w_c(\theta+\theta_1)\psi_R(-\theta_1,t)G_{R,1}(t)\\ &\quad+\gamma_D w_c(\theta+\theta_2)\psi_R(-\theta_2,t)G_{R,2}(t),\end{aligned} \tag{A.15}$$

$$\begin{aligned}\frac{\partial \psi_R(\theta,t)}{\partial t} &= -\psi_R(\theta,t)+\Phi_{Rl}(\theta,t)+\Phi_{Lc}(\theta,t)+\gamma_D w_l(\theta+\theta_1)\psi_R(-\theta_1,t)G_{R,1}(t)\\ &\quad+\gamma_D w_l(\theta+\theta_2)\psi_R(-\theta_2,t)G_{R,2}(t)+\gamma_D w_c(\theta-\theta_1)\psi_1(\theta_1,t)G_{L,1}(t)\\ &\quad+\gamma_D w_c(\theta-\theta_2)\psi_L(\theta_2,t)G_{L,2}(t)\end{aligned} \tag{A.16}$$

and

$$\begin{aligned}\frac{\partial \Phi_{Lm}(\theta,t)}{\partial t} &= -(\alpha^{-1}+\beta)\Phi_{Lm}(\theta,t)\\ &\quad-\beta(\gamma_D w_m(\theta-\theta_1)\psi_L(\theta_1,t)G_{L,1}(t)\Theta(\psi_L(\theta_1,t))\\ &\quad+\gamma_D w_m(\theta-\theta_2)\psi_L(\theta_2,t)G_{L,2}(t)\Theta(\psi_L(\theta_2,t))),\end{aligned} \tag{A.17}$$

$$\begin{aligned}\frac{\partial \Phi_{Rm}(\theta,t)}{\partial t} &= -(\alpha^{-1}+\beta)\Phi_{Rm}(\theta,t)\\ &\quad-\beta(\gamma_D w_m(\theta+\theta_1)\psi_R(-\theta_1,t)G_{R,1}(t)\Theta(\psi_R(-\theta_1,t))\\ &\quad+\gamma_D w_m(\theta+\theta_2)\psi_R(-\theta_2,t)G_{R,2}(t)\Theta(\psi_R(-\theta_2,t))),\end{aligned} \tag{A.18}$$

where $G_{L,j}(t)=G(\psi_L(\theta_j,t)), G_{R,j}(t)=G(\psi_R(-\theta_j,t))$, and

$$\begin{aligned}(\gamma_D)^{-1} &= |U_L'(\theta_k)|\\ &= \frac{1}{1+\alpha\beta}\left|w_l(\theta_k-\theta_1)-w_l(\theta_k-\theta_2)+w_c(\theta_k+\theta_2)-w_c(\theta_k+\theta_1)+I_L'(\theta_k)\right|\\ &= |U_R'(-\theta_k)|\\ &= \frac{1}{1+\alpha\beta}\left|w_l(\theta_k-\theta_2)-w_l(\theta_k-\theta_1)+w_c(\theta_k+\theta_1)-w_c(\theta_k+\theta_2)+I_R'(-\theta_k)\right|\end{aligned} \tag{A.19}$$

for $k=1,2$.

REFERENCES

[1] L. F. Abbott, J. A. Varela, K. Sen, and S. B. Nelson, *Synaptic depression and cortical gain control*, Science, 275 (1997), pp. 220–224.

[2] S. Amari, *Dynamics of pattern formation in lateral-inhibition type neural fields.*, Biol. Cybernet., 27 (1977), pp. 77–87.

[3] A. Angelucci, J. B. Levitt, E. J. S. Walton, J.-M. Hupe, J. Bullier, and J. S. Lund, *Circuits for local and global signal integration in primary visual cortex*, J. Neurosci., 22 (2002), pp. 8633–8646.

[4] E. Bart, S. Bao, and D. Holcman, *Modeling the spontaneous activity of the auditory cortex.*, J. Comput. Neurosci., 19 (2005), pp. 357–378.

[5] R. Ben-Yishai, R. L. Bar-Or, and H. Sompolinsky, *Theory of orientation tuning in visual cortex*, Proc. Natl. Acad. Sci. U.S.A., 92 (1995), pp. 3844–3848.
[6] R. Blake, *A primer on binocular rivalry, including current controversies*, Brain and Mind, 2 (2001), pp. 5–38.
[7] R. Blake and N. Logothetis, *Visual competition*, Nature Reviews Neuroscience, 3 (2002), pp. 1–11.
[8] G. G. Blasdel, *Orientation selectivity, preference, and continuity in monkey striate cortex*, J. Neurosci., 12 (1992), pp. 3139–61.
[9] C. J. Bossink, P. F. Stalmeier, and C. M. De Weert, *A test of Levelt's second proposition for binocular rivalry*, Vision Res., 33 (1993), pp. 1413–1419.
[10] J. W. Brascamp, R. van Ee, A. J. Noest, R. H. A. H. Jacobs, and A. V. van den Berg, *The time course of binocular rivalry reveals a fundamental role of noise*, J. Vision, 6 (2006), pp. 1244–1256.
[11] P. C. Bressloff and J. D. Cowan, *An amplitude equation approach to contextual effects in visual cortex*, Neural Comput., 14 (2002), pp. 493–525.
[12] P. C. Bressloff and Z. P. Kilpatrick, *Two–dimensional bumps in piecewise smooth neural fields with synaptic depression*, submitted.
[13] R. J. Brown and A. M. Norcia, *A method for investigating binocular rivalry in real-time with the steady state VEP*, Vision Res., 37 (1997), pp. 2401–2408.
[14] A. Buckthought, J. Kim, and H. R. Wilson, *Hysteresis effects in stereopsis and binocular rivalry*, Vis. Res., 48 (2010), pp. 819–830.
[15] F. S. Chance, S. B. Nelson, and L. F. Abbott, *Synaptic depression and the temporal response characteristics of* V1 *cells*, J. Neurosci., 18 (1998), pp. 4785–4799.
[16] B. Chapman, K. R. Zahs, and M. P. Stryker, *Relation of cortical cell orientation selectivity to alignment of receptive fields of the geniculocortical afferents that arborize within a single orientation column in ferret visual cortex*, J. Neurosci., 11 (1991), pp. 1347–1358.
[17] S. C. Chong, D. Tadin, and R. Blake, *Endogenous attention prolongs dominance durations in binocular rivalry*, J. Vision, 5 (2005), pp. 1004–1012.
[18] S. Coombes and M. R. Owen, *Evans functions for integral neural field equations with Heaviside firing rate function*, SIAM J. Appl. Dyn. Syst., 3 (2004), pp. 574–600.
[19] S. Coombes, *Waves, bumps, and patterns in neural field theories*, Biol. Cybernet., 93 (2005), pp. 91–108.
[20] R. Curtu, A. Shpiro, N. Rubin, and J. Rubin, *Mechanisms for frequency control in neuronal competition models*, 7 (2008), pp. 609–649.
[21] M. di Bernardo, C. J. Budd, A. R. Champneys, and P. Kowalczyk, *Piecewise-Smooth Dynamical Systems: Theory and Applications*, Springer, London, 2008.
[22] O. Faugeras, R. Veltz, and F. Grimbert, *Persistent neural states: Stationary localized activity patterns in the nonlinear continuous n-population, q-dimensional neural networks*, Neural Comput., 21 (2009), pp. 147–187.
[23] D. Ferster and K. D. Miller, *Neural mechanisms of orientation selectivity in the visual cortex*, Ann. Rev. Neurosci., 23 (2000), pp. 441–471.
[24] R. Fox and F. Rasche, *Binocular rivalry and reciprocal inhibition*, Percept. Psychophys., 5 (1969), pp. 215–217.
[25] A. W. Freeman, *Multistage model for binocular rivalry*, J. Neurophysiol., 94 (2005), pp. 4412–4420.
[26] C. D. Gilbert, *Horizontal integration and cortical dynamics*, Neuron, 9 (1992), pp. 1–13.
[27] Y. Guo and C. C. Chow, *Existence and stability of standing pulses in neural networks:* II. *Stability*, SIAM J. Appl. Dyn. Syst., 4 (2005), pp. 249–281.
[28] J. D. Haynes, R. Deichman, and G. Rees, *Eye-specific effects of binocular rivalry in the human lateral geniculate nucleus*, Nature, 438 (2005), pp. 496–499.
[29] H. von Helmholtz, *Treatise on Physiological Optics*, Dover, New York, 1866.
[30] J. C. Horton and D. L. Adams, *The cortical column: A structure without a function*, Proc. R. Soc. London B Biol. Sci., 360 (2005), pp. 837–862.
[31] D. H. Hubel and T. N. Wiesel, *Receptive fields, binocular interaction and functional architecture in the cat's visual cortex*, J. Physiol., 160 (1962), pp. 106–154.
[32] D. H. Hubel and T. N. Wiesel, *Ferrier lecture. functional architecture of macaque monkey visual cortex*, Proc. R. Soc. London B Biol. Sci., 198 (1977), pp. 1–59.

[33] J. M. Ichida and V. A. Casagrande, *Organization of the feedback pathway from striate cortex (V1) to the lateral geniculate nucleus (LGN) in the owl monkey (Aotus trivirgatus)*, J. Comp. Neurol., 454 (2002), pp. 272–283.
[34] D. Z. Jin, V. Dragoi, M. Sur, and H. S. Seung, *Tilt aftereffect and adaptation-induced changes in orientation tuning and visual cortex*, J. Neurosci., 94 (2005), pp. 4038–4050.
[35] L. C. Katz, C. D. Gilbert, and T. N. Wiesel, *Local circuits and ocular dominance columns in monkey striate cortex*, J. Neurosci., 9 (1989), pp. 1389–1399.
[36] Z. P. Kilpatrick and P. C. Bressloff, *Effects of adaptation and synaptic depression on spatiotemporal dynamics of an excitatory neuronal network*, Phys. D, 239 (2010), pp. 547–560.
[37] Z. P. Kilpatrick and P. C. Bressloff, *Stability of bumps in piecewise smooth neural fields with nonlinear adaptation*, Phys. D, 239 (2010), pp. 1048–1060.
[38] L. Lack, *Selective Attention and the Control of Binocular Rivalry*, Mouton, The Hague, 1978.
[39] C. R. Laing and C. C. Chow, *A spiking neuron model for binocular rivalry*, J. Comput. Neurosci., 12 (2002), pp. 39–53.
[40] S.-H. Lee, R. Blake, and D. J. Heeger, *Traveling waves of activity in primary visual cortex during binocular rivalry*, Nat. Neurosci., 8 (2004), pp. 22–23.
[41] S. R. Lehky, *An astable multivibrator model of binocular rivalry*, Perception, 17 (1988), pp. 215–228.
[42] S. R. Lehky, *Binocular rivalry is not chaotic*, Proc. Roy. Soc. London: Biol. Sci., 259 (1995), pp. 71–76.
[43] S. R. Lehky, *No binocular rivalry in the LGN of alert macaque monkeys*, Vis. Res., 36 (1996), pp. 1225–1234.
[44] D. A. Leopold and N. K. Logothetis, *Activity changes in early visual cortex reflect monkeys' percepts during binocular rivalry*, Nature, 379 (1996), pp. 549–553.
[45] W. J. M. Levelt, *On Binocular Rivalry*, Institute for Perception RVO–TNO, Soesterberg, The Netherlands, 1965.
[46] N. K. Logothetis, D. A. Leopold, and D. L. Sheinberg, *What is rivalling during binocular rivalry?*, Nature, 380 (1996), pp. 621–624.
[47] P. N. Loxley and P. A. Robinson, *Soliton model of competitive neural dynamics during binocular rivalry*, Phys. Rev. Lett., 102 (2009), 258701.
[48] R. S. Menon, S. Ogawa, J. P. Strupp, and K. Uğurbil, *Ocular dominance in human v1 demonstrated by functional magnetic resonance imaging*, J. Neurophysiol., 77 (1997), pp. 2780–2787.
[49] R. Moreno-Bote, J. Rinzel, and N. Rubin, *Noise-induced alternations in an attractor network model of perceptual bistability*, J. Neurophysiol., 98 (2007), pp. 1125–1139.
[50] D. J. Pinto and G. B. Ermentrout, *Spatially structured activity in synaptically coupled neuronal networks:* II. *Lateral inhibition and standing pulses*, SIAM J. Appl. Math., 62 (2001), pp. 226–243.
[51] A. Polonsky, R. Blake, J. Braun, and D. J. Heeger, *Neuronal activity in human primary visual cortex correlates with perception during binocular rivalry*, Nat. Neurosci., 3 (2000), pp. 1153–1159.
[52] A. Shpiro, R. Curtu, J. Rinzel, and N. Rubin, *Dynamical characteristics common to neuronal competition models*, J. Neurophysiol., 97 (2007), pp. 462–73.
[53] A. Shpiro, R. Moreno-Bote, N. Rubin, and J. Rinzel, *Balance between noise and adaptation in competition models of perceptual bistability*, J. Comput. Neurosci., 27 (2009), pp. 37–54.
[54] F. K. Skinner, N. Kopell, and E. Marder, *Mechanisms for oscillation and frequency control in reciprocally inhibitory model neural networks*, J. Comput. Neurosci., 1 (1994), pp. 69–87.
[55] L. Sincich and G. Blasdel, *Oriented axon projections in primary visual cortex of the monkey*, J. Neurosci., 21 (2001), pp. 4416–4426.
[56] M. Stocker, M. Krause, and P. Pedarzani, *An apamin-sensitive Ca^{2+}-activated K^+ current in hippocampal pyramidal neurons*, Proc. Natl. Acad. Sci. U.S.A., 96 (1999), pp. 4662–4667.
[57] J. Tabak, W. Senn, M. J. O'Donovan, and J. Rinzel, *Modeling of spontaneous activity in developing spinal cord using activity-dependent depression in an excitatory network*, J. Neurosci., 20 (2000), pp. 3041–3056.
[58] A. L. Taylor, G. W. Cottrell, and W. B. Kristan, Jr., *Analysis of oscillations in a reciprocally inhibitory network with synaptic depression*, Neural Comput., 14 (2002), pp. 561–581.
[59] F. Tong and S. A. Engel, *Interocular rivalry revealed in the human cortical blind-spot representation*, Nature, 411 (2001), pp. 195–199.

[60] F. Tong, M. Meng, and R. Blake, *Neural bases of binocular rivalry*, Trends in Cog. Sci., 10 (2006), pp. 502–511.
[61] R. B. Tootell, E. Switkes, M. S. Silverman, and S. L. Hamilton, *Functional anatomy of macaque striate cortex.* II. *Retinotopic organization*, J. Neurosci., 8 (1988), pp. 1531–1568.
[62] M. Tsodyks, K. Pawelzik, and H. Markram, *Neural networks with dynamic synapses*, Neural Comput., 10 (1998), pp. 821–835.
[63] J. A. Varela, K. Sen, J. Gibson, J. Fost, L. F. Abbott, and S. B. Nelson, *A quantitative description of short-term plasticity at excitatory synapses in layer* 2/3 *of rat primary visual cortex*, J. Neurosci., 17 (1997), pp. 7926–7940.
[64] N. J. Wade and P. Wenderoth, *The influence of colour and contour rivalry on the magnitude of the tilt aftereffect*, Vis. Res., 18 (1978), pp. 827–835.
[65] X. J. Wang and J. Rinzel, *Alternating synchronous rhythms in reciprocally inhibitory model neurons*, Neural Comput., 4 (1992), pp. 84–97.
[66] H. R. Wilson, *Computational evidence for a rivalry hierarchy in vision*, Proc. Natl. Acad. Sci. U.S.A., 100 (2003), pp. 14499–14503.
[67] H. R. Wilson, R. Blake, and S. H. Lee, *Dynamics of travelling waves in visual perception*, Nature, 412 (2001), pp. 907–910.
[68] H. R. Wilson and J. D. Cowan, *Excitatory and inhibitory interactions in localized populations of model neurons*, Biophys. J., 12 (1972), pp. 1–24.
[69] L. C. York and M. C. W. van Rossum, *Recurrent networks with short term synaptic depression*, J. Comput. Neurosci., 27 (2009), pp. 607–620.